

Supporting information

On/off porosity switching and post-assembly modifications of Cu₄L₄ metal-organic polyhedra

Witold M. Bloch,^{*a} Ravichandar Babarao^{b,c} and Matthew L. Schneider^a

^aDepartment of Chemistry, The University of Adelaide, Adelaide, Australia.

^bSchool of Science, RMIT University, Melbourne, Victoria 3001, Australia.

^cCSIRO, Normanby Road, Clayton 3168, Victoria, Australia.

Table of contents

1. Experimental section	3
1.2. Materials and measurements	3
1.3. Synthesis of LH ₂	3
1.3.1. Synthesis of methyl 3-ethynylbenzoate (4)	3
1.3.2. Synthesis of compound 5	4
1.3.3. Synthesis of LH ₂	4
1.4. Synthesis of 1a-e , 2 and 3	5
1.4.1. Synthesis of 1a	5
1.4.2. Post-synthetic modification of 1	8
2. Powder X-ray diffraction	9
3. Thermal gravimetric analysis (TGA)	15
4. Gas adsorption	17
5. X-ray crystallography	18
4.1. General methods	18
3.1.1. Specific refinement details for 1a and 1c	18
3.1.2. Specific refinement details for 1b	18
3.1.5. Specific refinement details for 1d	19
3.1.4. Specific refinement details for 1e	19
3.1.6. Specific refinement details for 2	19
3.1.7. Specific refinement details for 3	19
5.2. Thermal ellipsoid plots	21
5.3. Additional information on 1a-e	23
6. Lattice energy calculations	24
7. References	27

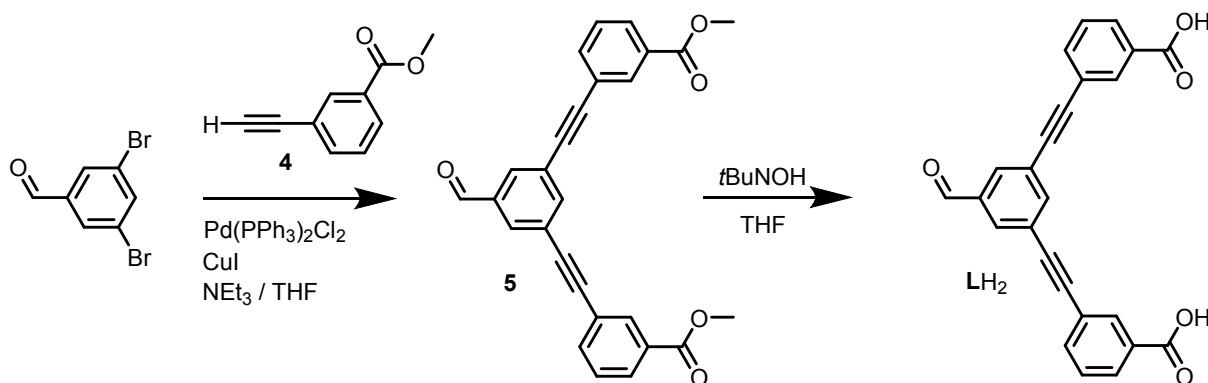
1. Experimental section

1.2. Materials and measurements

Unless otherwise stated, all chemicals were obtained from commercial sources and used as received. Triethyl amine (NEt_3) was distilled from KOH and stored under argon. Tetrahydrofuran (THF) was freshly distilled using a sodium/benzophenone solvent still. Electrospray ionization (ESI) mass spectra were recorded on an Agilent 6230 TOF LCMS. Elemental analyses were performed by the microanalysis laboratory at Macquarie University. Infrared spectra were collected on a Perkin-Elmer Spectrum 100 using a UATR sampling accessory. Thermal gravimetric analysis (TGA) was performed on a Perkin-Elmer STA-6000 instrument or on a TA Instruments Discovery TGA under a constant flow of N_2 at a temperature increase rate of $10\text{ }^\circ\text{C}/\text{min}$.

Powder X-ray diffraction data were collected on a Bruker Advance D8 diffractometer (capillary stage) using Cu K α radiation ($\lambda = 1.5418\text{ \AA}$, 50 kW/40mA). 1.0 mm capillaries were filled with the respective solvent before loading crystals of **1-3**. This was done to avoid any possible desolvation of the crystalline sample. Simulated powder X-ray diffraction patterns were generated from the single crystal data using Mercury 3.10. Data in figure S14b was collected on a Co-target Bruker D4 Endeavour powder diffractometer (plate stage). The data was converted to Cu wavelength using PowDLL. Gas sorption isotherm measurements were performed on a Micromeritics 3Flex Surface Characterisation Analyser. UHP grade (99.999 %) N_2 was used for all measurements. Temperatures were maintained at 77 K using a cryo-cooler. The isotherms were then analysed to determine the Brunauer Emmett-Teller (BET) surface area and pore-size distribution using the MicroActive software (Version 3.00, Micromeritics Instrument Corp. 2013).

1.3. Synthesis of LH_2



Scheme 1

1.3.1. Synthesis of methyl 3-ethynylbenzoate (**4**)

Methyl 3-bromobenzoate (2.98 g, 13.9 mmol) was dissolved in triethylamine (30 mL) under argon atmosphere. Once the solvent was degassed, $\text{Pd}(\text{PPh}_3)_2\text{Cl}_2$ (207 mg, 0.29 mmol) and CuI (60.1 mg, 0.31 mmol) were added in one portion, followed by ethynyltrimethylsilane (5.0 mL, 36.1 mmol). The reaction mixture was sealed and heated at $65\text{ }^\circ\text{C}$ for 18 h. Once allowed to cool, the reaction mixture was diluted with ethyl acetate (30 mL), filtered, and concentrated under reduced pressure. The residue was purified by column chromatography (3:1 hexane/ CH_2Cl_2) to yield a pale-yellow oil. ^1H NMR (500 MHz, CDCl_3): δ 8.14 (d, $J = 1.7\text{ Hz}$, 1H), 7.97 (dt, $J = 7.7, 1.4\text{ Hz}$, 1H), 7.63 (dt, $J = 7.7, 1.4\text{ Hz}$, 1H), 7.38 (t, $J = 7.7\text{ Hz}$, 1H), 3.92 (s, 3H), 0.26 (s, 9H). K_2CO_3 (1.80 g) was added to the oil in methanol (45 mL) and the suspension was stirred at $25\text{ }^\circ\text{C}$ for 2 h. Diethyl ether (50 mL) was added and the suspension was filtered. Water (75 mL) was added and the organic layer was separated and the aqueous layer was further extracted with diethyl ether (3 x 30 mL). The combined extracts were dried over MgSO_4 and the solvent was evaporated under reduced pressure, yielding an off-white solid (1.8 g, 81%). ^1H NMR (500 MHz, CDCl_3): δ 8.22 – 8.13 (d, $J = 1.8\text{ Hz}$, 1H), 8.02 (dd, $J = 7.7, 1.8\text{ Hz}$, 1H), 7.67 (dd, $J = 7.7, 1.8\text{ Hz}$, 1H), 7.41 (t, $J = 7.7$, 1H), 3.93 (s, 3H), 3.12 (s, 1H). ^{13}C NMR (125 MHz, CDCl_3) δ 166.40, 136.38, 133.41, 130.64, 129.94, 128.62, 122.74, 82.71, 78.26, 52.44.

1.3.2. Synthesis of compound 5

3,5-Dibromobenzaldehyde (177 mg, 0.747 mmol) was combined with compound 4 (263 mg, 1.64 mmol) in triethylamine (6 mL) and THF (2 mL) under an argon atmosphere. After the solvent was degassed, Pd(PPh₃)₂Cl₂ (12.0 mg, 0.017 mmol) and CuI (3.4 mg, 0.018 mmol) were added in one portion and the reaction mixture was heated at 75 °C for 18 h. Once allowed to cool, the reaction mixture was diluted with ethyl acetate (10 mL), filtered, and concentrated under reduced pressure. The residue was purified by column chromatography (CH₂Cl₂), yielding dimethyl 3,3'-((5-formyl-1,3-phenylene)bis(ethyne-2,1-diyl))dibenzoate (**5**) as a pale brown solid (283 mg, 78%). Mp: 139.0 – 140.5 °C ¹H NMR (500 MHz, CDCl₃): δ 10.02 (s, 1H), 8.23 (t, *J* = 1.7 Hz, 2H), 8.04 (dt, *J* = 7.7, 1.7 Hz, 2H), 8.00 (d, *J* = 1.6 Hz, 2H), 7.94 (d, *J* = 1.6 Hz, 1H), 7.72 (dt, *J* = 7.7, 1.7 Hz, 2H), 7.47 (t, *J* = 7.7 Hz, 2H), 3.95 (s, 6H). ¹³C NMR (125 MHz, CDCl₃) δ 190.76, 166.38, 139.71, 136.89, 135.91, 133.07, 132.32, 130.77, 130.00, 128.81, 124.74, 123.01, 90.64, 88.06, 52.51; *v*_{max} (neat, cm⁻¹): 3568 (m), 1717 (s), 1701 (s), 1590 (m), 1483 (m), 1443 (m). ESI-HRMS (C₂₇H₁₈O₅): calc: 445.1046 [M+Na]⁺; found 445.1046.

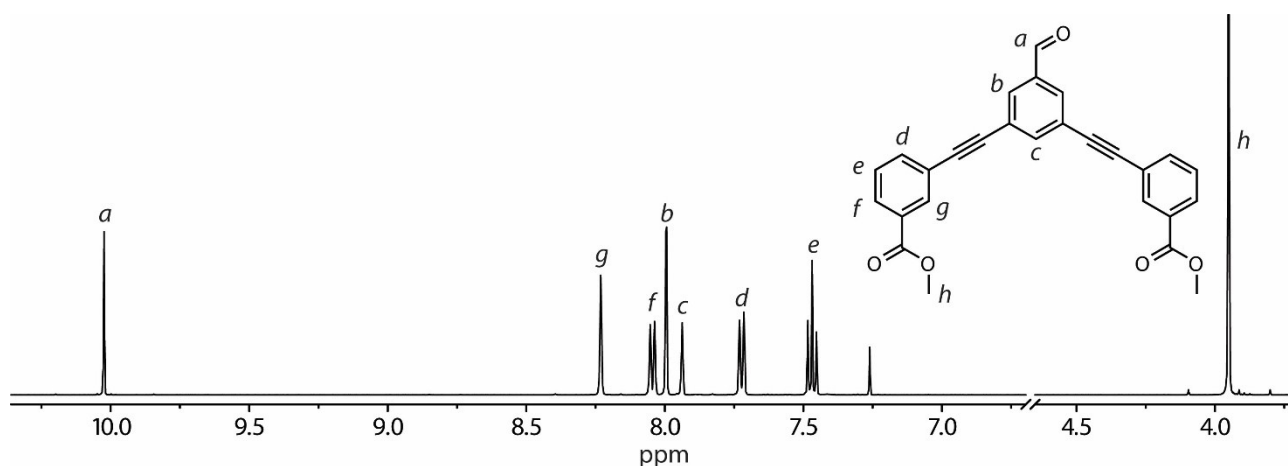


Figure S1. ¹H NMR spectrum (500 MHz/CDCl₃) of compound 5.

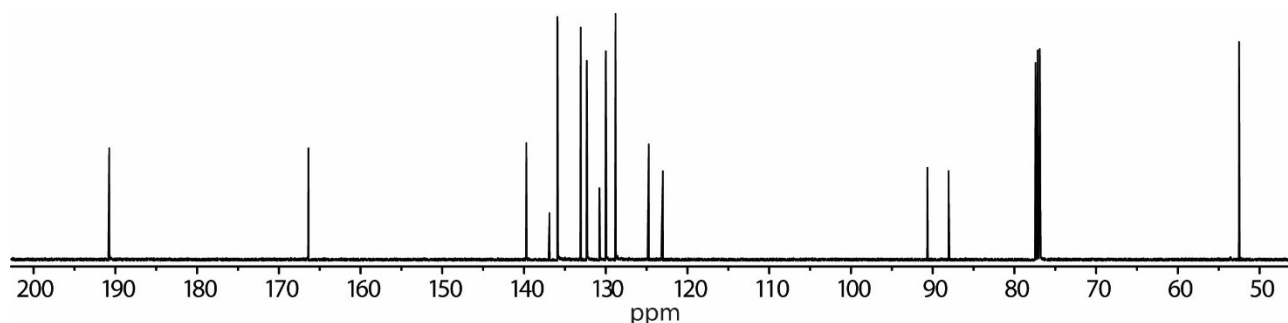


Figure S2. ¹³C NMR spectrum (125 MHz/ CDCl₃) of compound 5.

1.3.3. Synthesis of LH₂

Tetrabutylammonium hydroxide (1M in methanol, 1.8 mL, 1.8 mmol, 4 equiv.) was combined with compound 5 (190 mg, 0.450 mmol) in dry THF (8 mL) and the mixture was stirred at 25 °C for 2 h. The volatiles were removed under an N₂ stream and the residue was acidified to pH = 3 with 1M HCl. The formed precipitate was collected under reduced pressure washing thoroughly with H₂O. The wet solid was then washed with MeOH (2 x 10 mL) and dried under vacuum (18 h) to give 3,3'-((5-formyl-1,3-phenylene)bis(ethyne-2,1-diyl))dibenzoic acid (LH₂) as a white solid (145 mg, 82%). Mp: >260 °C. ¹H NMR (600 MHz, DMSO-*d*₆) δ 13.30 (s, 2H), 10.05 (s, 1H), 8.16 (d, *J* = 1.6 Hz, 1H), 8.16 – 8.13 (m, 4H), 8.01 (dd, *J* = 7.7, 1.4 Hz, 2H), 7.86 (dt, *J* = 7.7, 1.4 Hz, 2H), 7.61 (t, *J* = 7.7 Hz, 2H). ¹³C NMR (151 MHz, DMSO-*d*₆) δ 191.97, 166.47, 139.12, 136.98, 135.57, 132.30, 132.19, 131.50, 129.99, 129.42, 123.69, 122.04, 90.30, 87.94. *v*_{max} (neat, cm⁻¹): 2810 (w), 1686 (br, s), 1602 (m), 1589 (m), 1484 (w), 1453 (m). ESI-HRMS (C₂₅H₁₄O₅): calc: 394.0847 [M-H]⁻; found 394.0829.

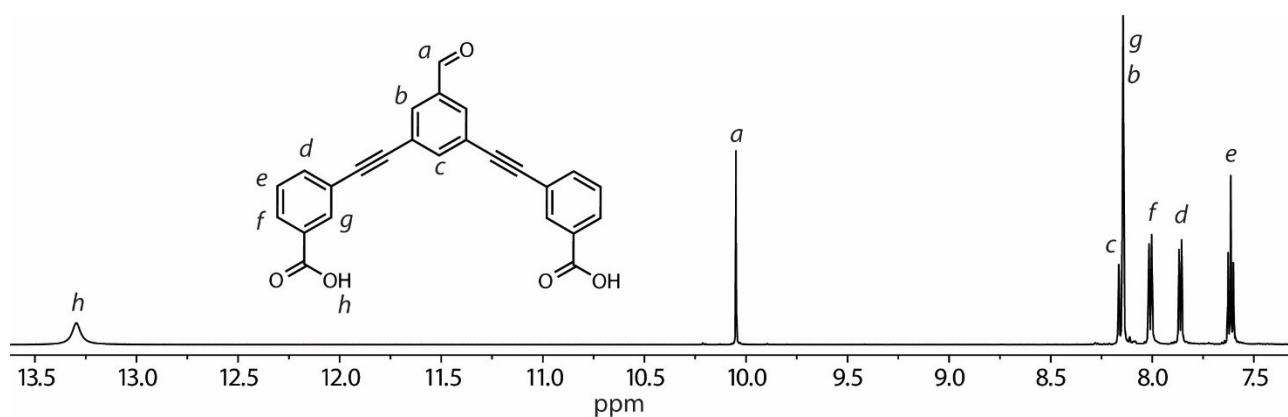


Figure S3. ^1H NMR spectrum (600 MHz/ DMSO) of compound LH_2 .

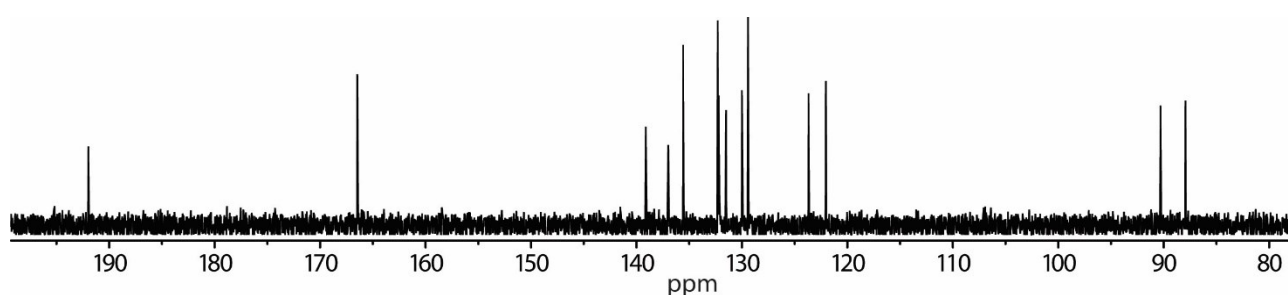


Figure S4. ^{13}C NMR spectrum (125 MHz/ DMSO) of LH_2 .

1.4. Synthesis of **1a-e**, **2** and **3**.

1.4.1. Synthesis of **1a**

In a screw-cap vial **L** (60 mg, 0.15 mmol) was combined with $\text{Cu}(\text{OAc})_2 \cdot \text{H}_2\text{O}$ (40 mg, 0.20 mmol) in 4.5 mL of (DMF). The vial was placed in an oven pre-set to 85 °C and left to stand for 2 h. After allowing to cool to room temperature, the resulting blue solution of **1** was subject to crystallisation conditions outlined in table 1. Slow vapour diffusion of MeOH (2 mL) into the DMF solution of **1** (0.5 mL) gave blue crystals after 4 days. The crystals were soaked in MeOH (x 7) over 24 hrs and isolated under reduced pressure (Yield 65 mg, 87%, based on analysis). ν_{max} (neat, cm^{-1}): 1697.4 (m, HC=O), 1629.3 (m), 1594.9 (m), 1572.8 (m), 1431.3 (m), 1394.9 (s). Found: C 61.58 H 3.45 $\text{C}_{102}\text{H}_{68}\text{Cu}_4\text{O}_{28}$ ($[\text{Cu}_4\text{L}_4(\text{MeOH})_2(\text{H}_2\text{O})_2] \cdot 4\text{H}_2\text{O}$) requires: C 61.38 H 3.43.

Table S1: Crystallisation condition employed to obtain phases **1a-e**

Solvents x/y; slow-vapour diffusion of y into x	Crystallised phase
DMF/MeOH	1a
DMF/ CH_3CN	1a
DMSO ^b	1b
DMA/MeOH	1b
DMF/ether	1c
DMF/acetone	1c
DMF/ H_2O ^a	1c
DMA/ether	1d
DMA/ H_2O ^a	1d
Acetone ^c	1e

^a Vial was left open to the air; ^b crystals formed upon heating LH_2 and $\text{Cu}(\text{OAc})_2$ at 85 °C for 16 h; ^c Crystals of **1c** were washed with acetone (x4) and left to soak for 3 weeks at 25 °C.



Figure S5. A photo of dried samples of **1** dissolved in DMF (left) and DMA (right). Typical concentrations = 3.8 mM. Due to their solubility, phases **1a-1e** can be recycled through recrystallisation (Table S1).

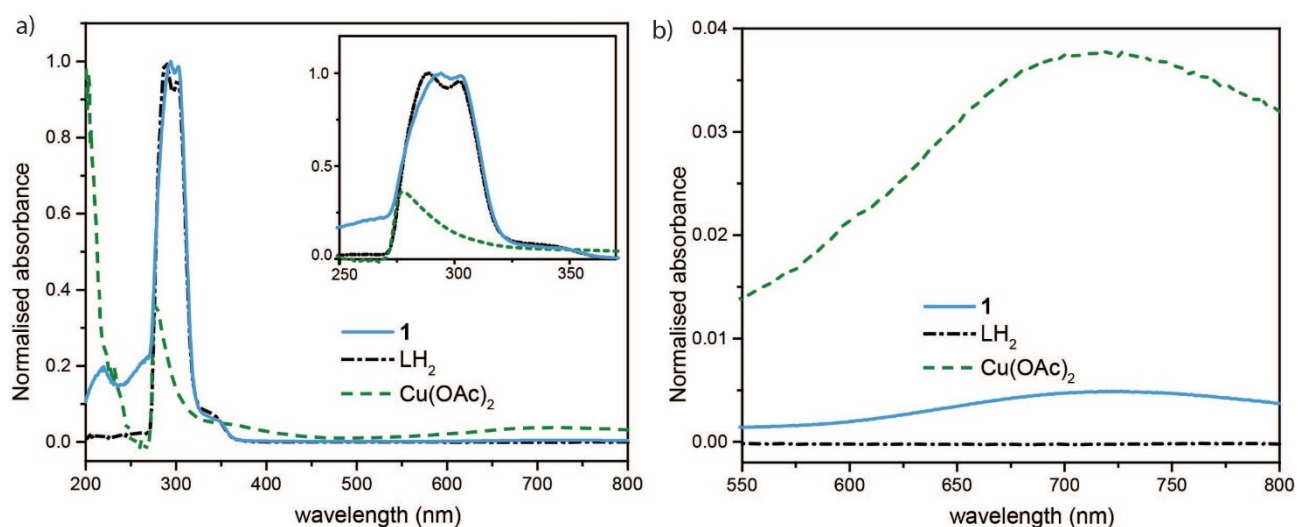


Figure S6. UV-Vis spectra of **1**, LH_2 and Cu(OAc)_2 measured in DMF at 25 °C. a) Overlay of LH_2 (dash-dot line, black), Cu(OAc)_2 (dashed line, green) and **1** (solid line, teal). Both LH_2 and **1** show similar features in the spectrum, however the high energy band observed in LH_2 (288 nm) is red-shifted in **1** (294 nm); b) the same spectrum shown between 550 – 800 nm, highlighting the d-d band characteristic of the copper paddlewheel node.¹

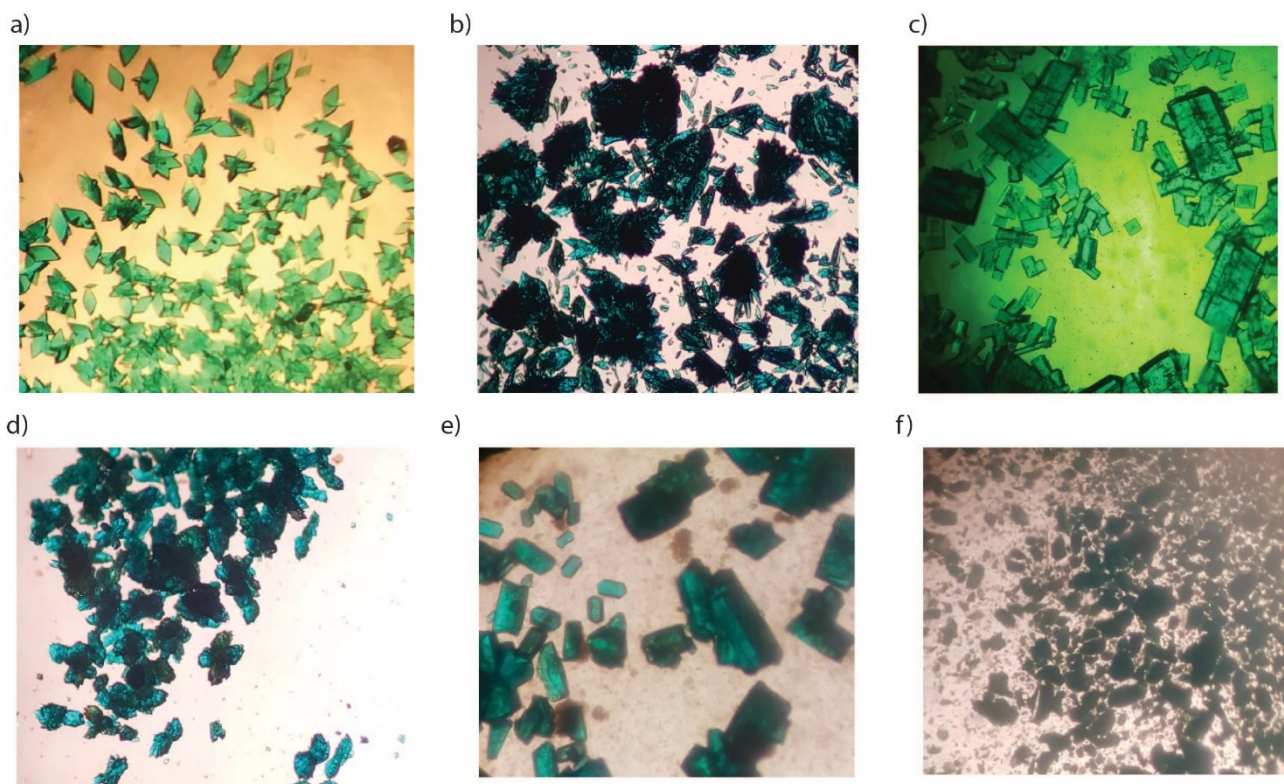


Figure S7. Images of the crystalline phases **1a-1e**; a) **1a**; b) **1b**; c) **1c**; d) **1e** (crystals shown in c) which have been soaked in acetone for 3 weeks); e) **1d**; f) the same sample shown in e) when exposed to in MeOH for 2 minutes. Photos were taken using a smartphone camera and crystals were visualised on a Meiji EMZ-13 microscope.

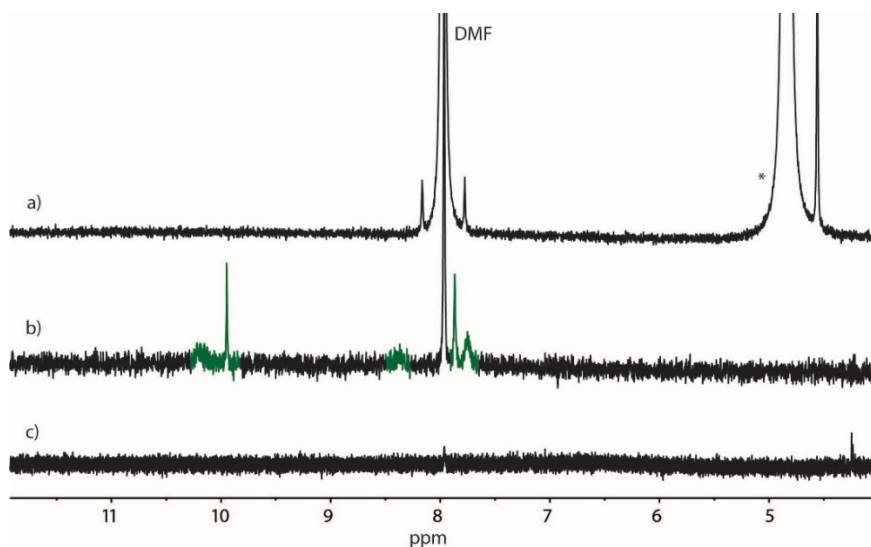


Figure S8. ^1H NMR spectra (500 MHz) of crystals of **1c** soaked in a) methanol- d_4 (1 wash). Note: the DMF signals originate from the coordinated solvent in **1c**. As can be observed, **1** is not soluble in MeOH even in the presence of DMF; b) acetone- d_6 (2 washes); c) acetone- d_6 4 washes. As can be observed, **1c** is soluble in acetone only in the presence of trace amounts of DMF. Similar results were observed for **1d**. After further washing with acetone, signals corresponding to **1** (indicated in green) disappear.

1.4.2. Post-synthetic modification of **1**

General procedure: in a 5 mm NMR tube, a dried powder of **1** (5 mg, ~2.7 μmol) was dissolved in 0.65 mL of DMF- d_7 with the aid of sonication and heating. Afterwards, 16 equivalents of the aniline derivative (o-toluidine or 3-Amino-9-ethylcarbazole) was added, followed by $\text{Sc}(\text{OTf})_3$ (~0.1 mg). The mixture was shaken and heated overnight at 45 $^\circ\text{C}$. Slow vapour diffusion of diethyl ether (2 mL) into the reaction mixture produced crystals suitable for X-ray analysis.

2: ν_{max} (neat, cm^{-1}): 1619.4 (m), 1594.3 (m), 1572.9 (m), 1484.9 (w)

3: ν_{max} (neat, cm^{-1}): 1630.0 (m), 1594.4 (m), 1571.3 (m), 1478.0 (m).

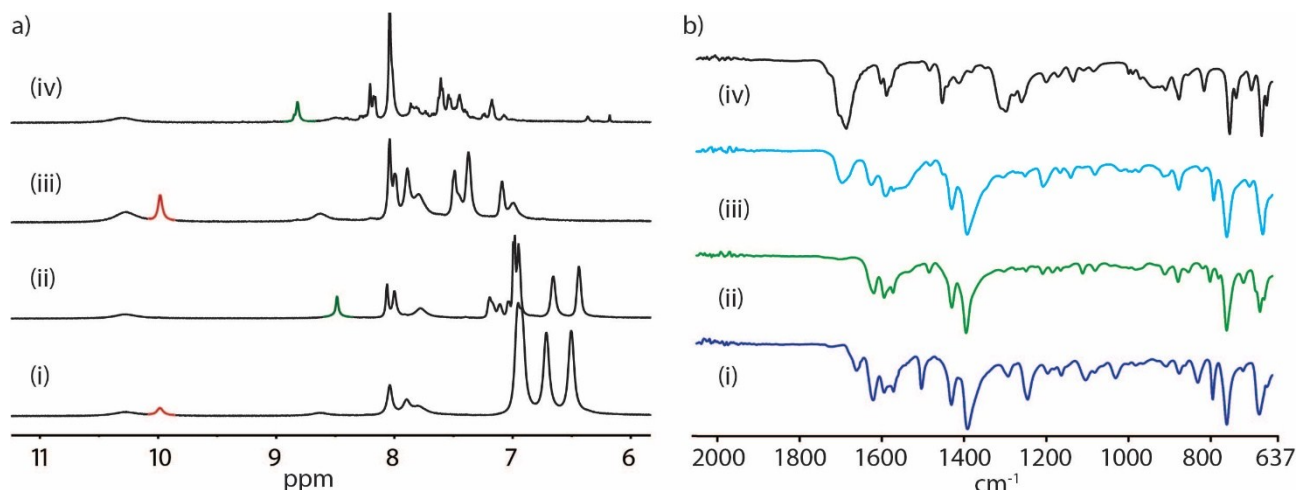


Figure S9. a) ^1H NMR (500 MHz/DMF- d_7) spectra of covalent PAM reactions (i) the mixture of **1** and o-toluidine before heating; (ii) the reaction mixture after addition of $\text{Sc}(\text{OTf})_3$ and heating at 45 $^\circ\text{C}$ /16 hrs; (iii) the mixture of **1** and 9-ethyl-9H-carbazol-3-amine before heating; (iv) the reaction mixture after addition of $\text{Sc}(\text{OTf})_3$ and heating at 45 $^\circ\text{C}$ /16 hrs. Both reaction mixtures show the absence of the aldehyde proton at ~10 ppm (red) and appearance a new imine proton (green) which appears between 8 and 9 ppm. (b) IR spectra of crystals of (i) **3**; (ii) **2**; (iii) **1**; (iv) ligand LH_2 . The success of the PAM reaction can be seen by the absence of the C=O aldehyde stretch at 1699 cm^{-1} and appearance of new C=N stretches.

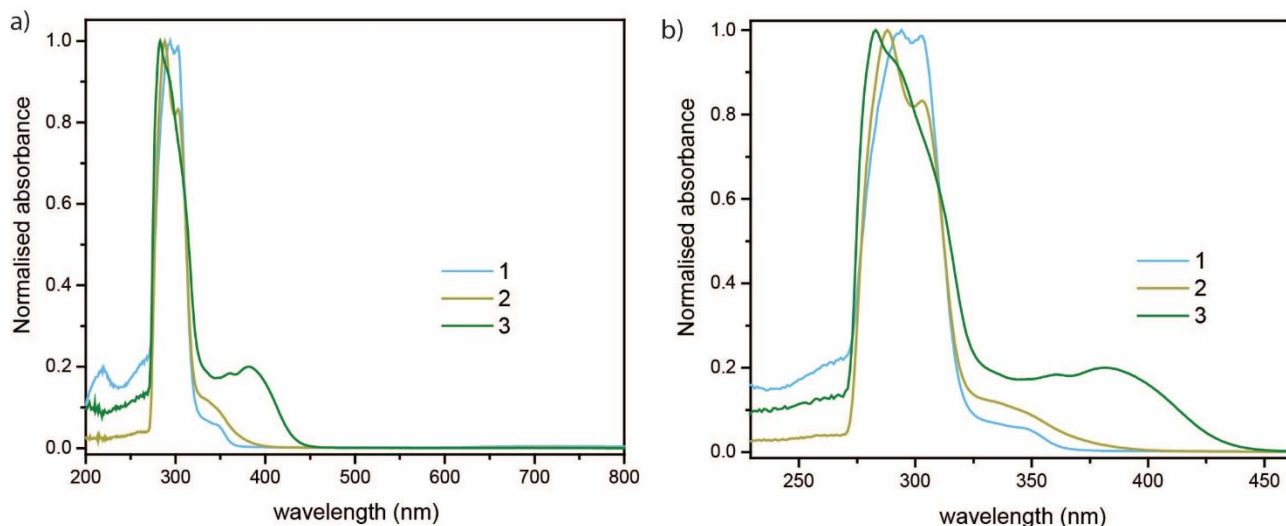


Figure S10. UV-Vis spectra of **1**, **2** and **3**, measured in DMF at 25 $^\circ\text{C}$ a) Full spectrum of **1** (blue line), **2** (khaki line) and **3** (green line); b) the same spectrum shown between 225 – 460 nm.

2. Powder X-ray diffraction

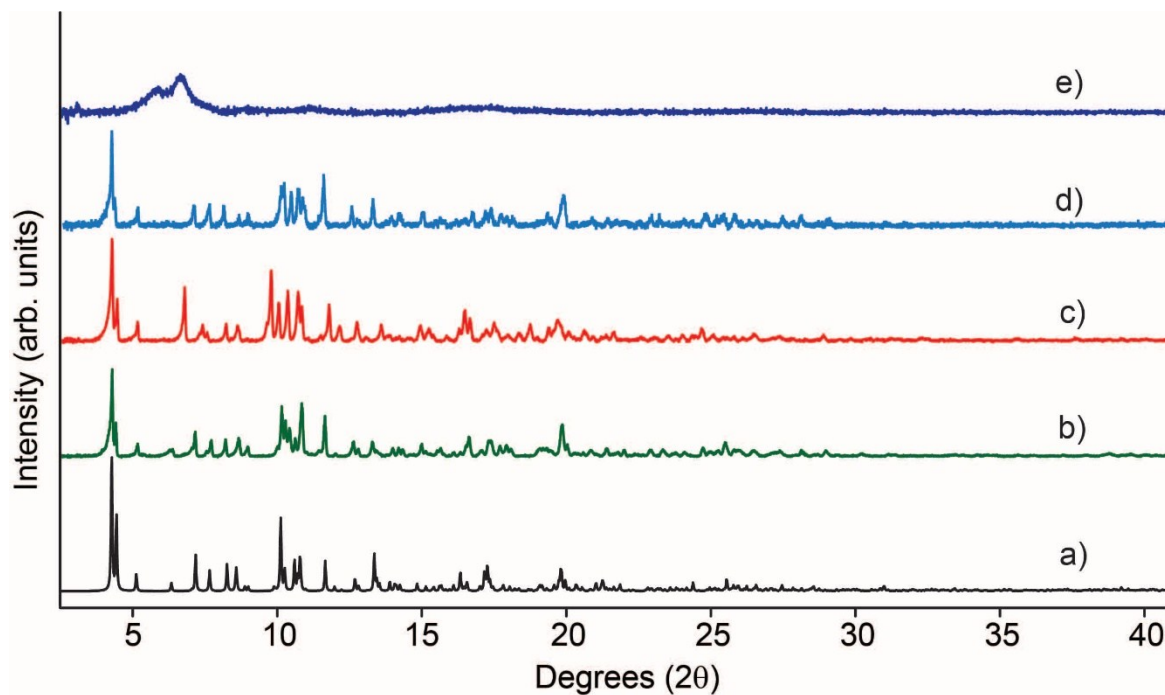


Figure S11. Powder X-ray diffraction patterns of **1a** showing solvent washing and activation: a) **1a** simulated; b) **1a** as-synthesised; c) **1a** acetone exchanged (soaked over 3 months); d) **1a** MeOH exchanged (over 6 hrs); e) **1a** activated sample. Note: minor discrepancies ($2\theta > 7^\circ$) are observed between a) – d) due to the overall flexibility of the MOP solid in accommodating different coordinating solvent molecules in the crystal lattice.

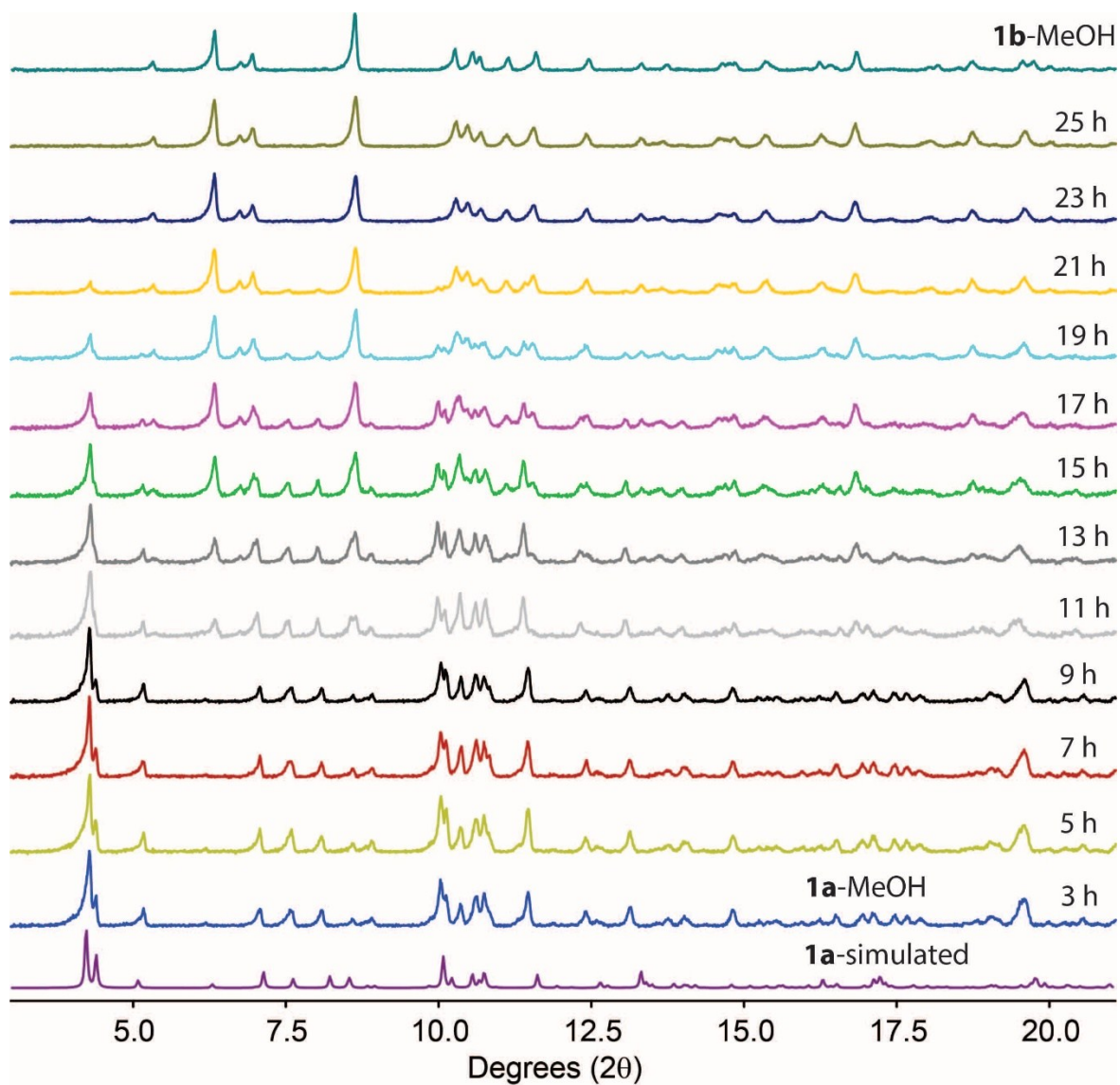


Figure S12. Powder X-ray diffraction patterns of **1a-MeOH** showing its metastability (up to 9 hrs) and subsequent slow conversion to give **1b-MeOH**. Note: **1a-MeOH** was prepared by exchanging an as-synthesised sample of **1a** with MeOH (5 x) over a period of 3 hrs. The sample was then loaded in a capillary filled with MeOH and measurements were performed every 2 hrs.

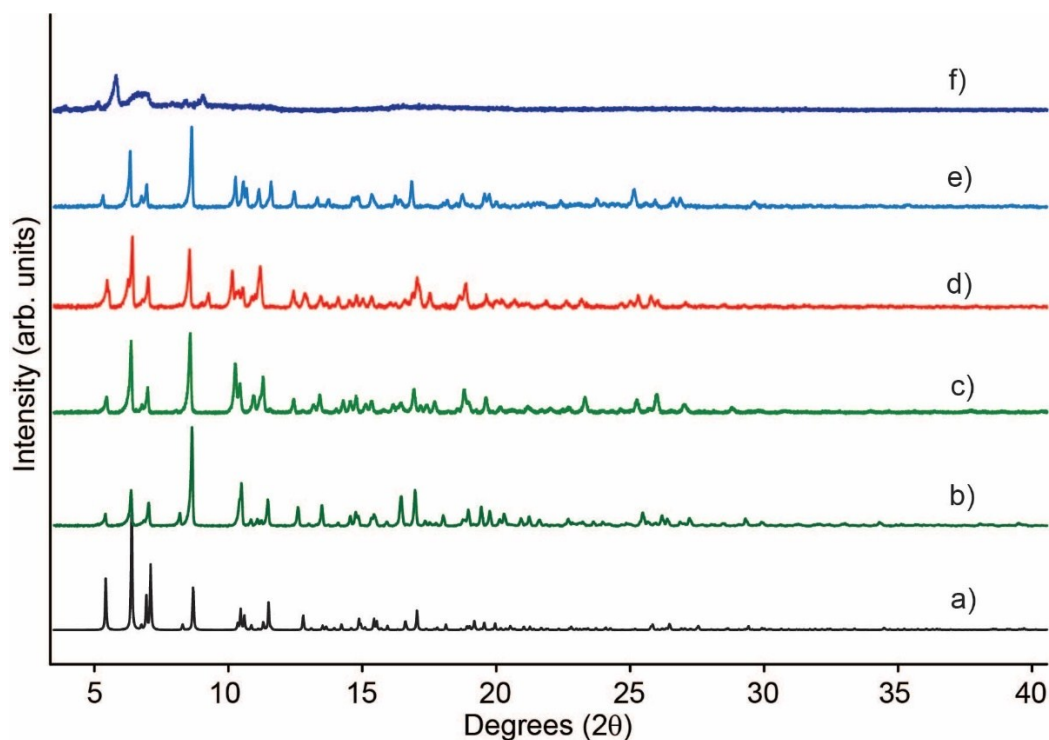


Figure S13. Powder X-ray diffraction patterns of **1b** showing solvent washing and activation: a) **1b-DMSO** simulated; b) **1b-DMSO** as-synthesised; c) **1b-DMA** as-synthesised, obtained from DMA/MeOH; d) **1b** acetone exchanged (soaked over 3 months); e) **1b** MeOH exchanged, f) **1b** activated sample.

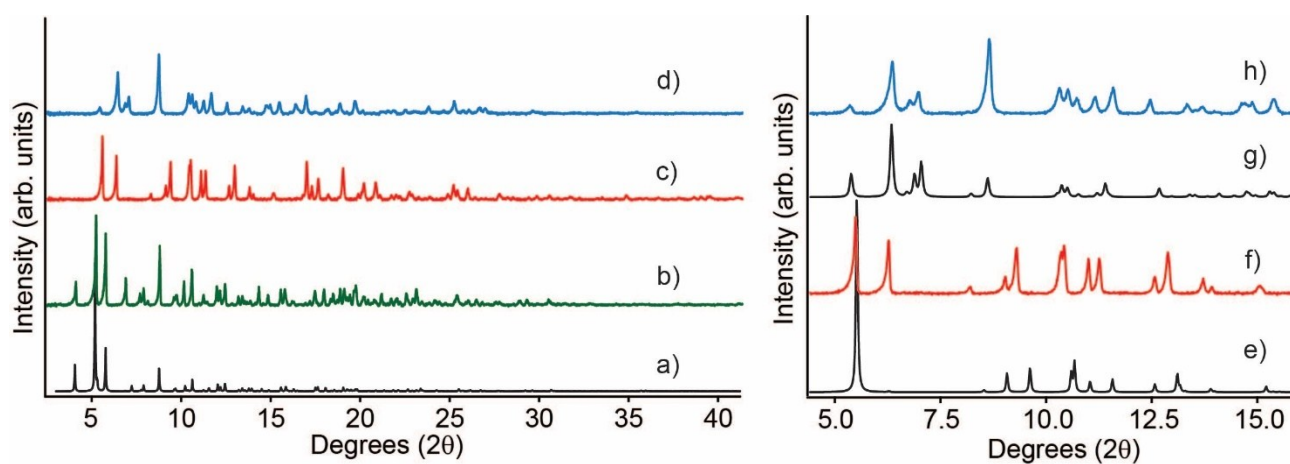


Figure S14. Powder X-ray diffraction patterns of **1c** showing solvent washing and transformations; a) **1c** simulated; b) **1c** as-synthesised; c) **1c** soaked in acetone for 3 weeks; d) **1c** soaked in MeOH for 5 minutes; e) **1e** simulated pattern; f) the same pattern as shown in c); g) **1b** simulated; h) the same pattern as shown in d). As can be seen in e) – h), **1c** transforms to **1e** or **1b** upon exposure of the crystals to acetone or MeOH respectively.

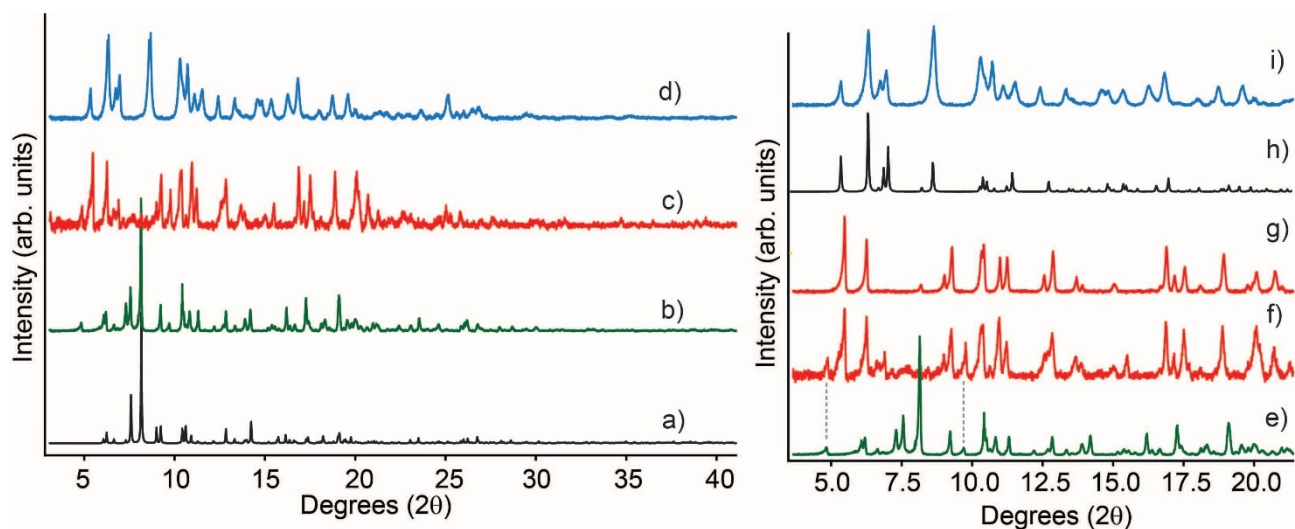


Figure S15. Powder X-ray diffraction patterns of **1d** showing solvent washing and transformations; a) **1d** simulated; b) **1d** as-synthesised; c) **1d** soaked in acetone for 3 weeks; d) **1d** soaked in MeOH for 5 minutes; e) **1d** as-synthesised; f) the same pattern as shown in c); g) **1e** as-synthesised, obtained by exposing **1c** to acetone (shown for comparison); h) **1b** simulated; i) the same pattern as shown in d). As can be seen in e) – h), **1d** transforms to **1e** or **1b** upon exposure of the crystals to acetone or MeOH respectively. We note that the conversion to **1e** does not proceed as cleanly as the same transformation from **1c**. The diffraction peaks at $2\theta = 4.9$ and 9.8 suggest the presence of the parent phase **1d** in the transformed sample.

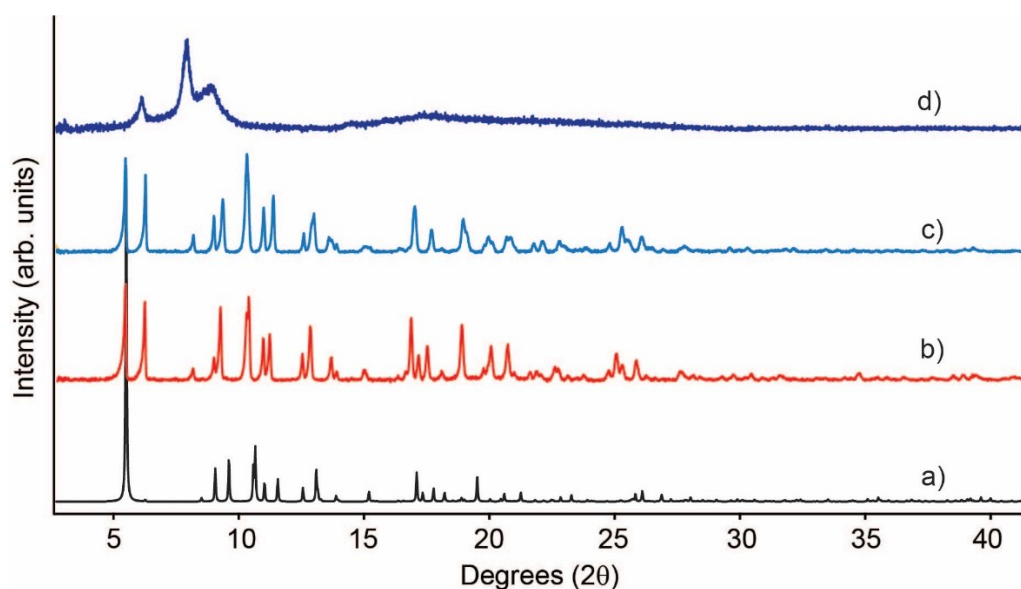


Figure S16. Powder X-ray diffraction patterns of **1e** showing solvent washing and activation: **1e** simulated; b) **1e** as-synthesised (**1c** recrystallised from acetone); c) **1e** MeOH exchanged, f) **1e** activated sample.

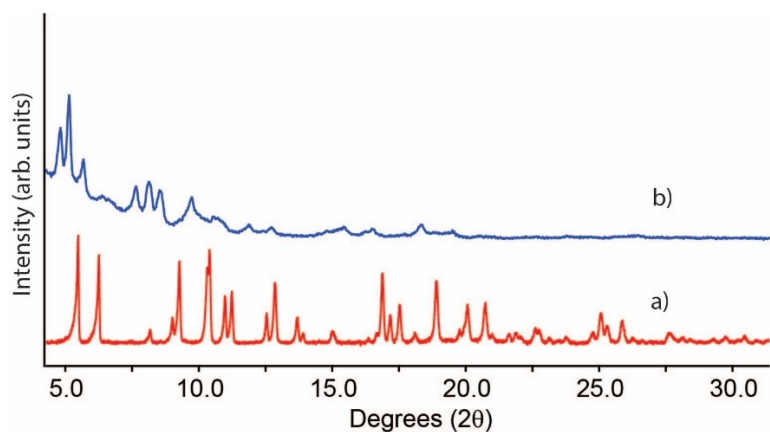


Figure S17. Powder X-ray diffraction patterns of a) **1e** as-synthesized (obtained from the slow recrystallisation of **1c** in acetone); b) the solid obtained by heating and stirring equimolar amounts of **L** + $\text{Cu}(\text{OAc})_2$ in acetone at 60 °C for 2h. The pattern in b) does not coincide with **1a-e**.

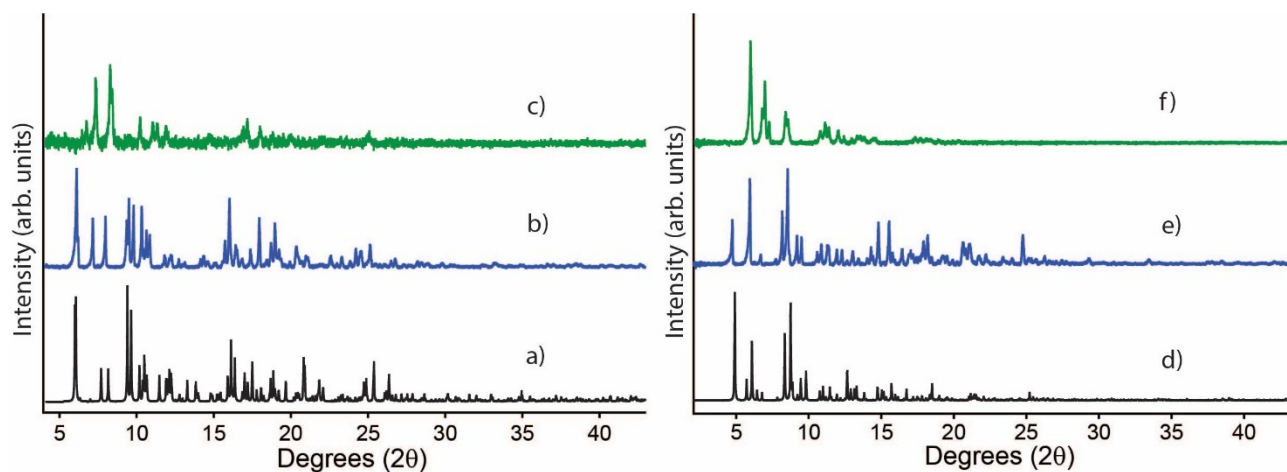


Figure S18. Powder X-ray diffraction patterns of PAM structures **2** and **3**; a) **2** simulated; b) **2** as-synthesized; c) **2** desolvated; d) **3** simulated; e) **3** as-synthesized; f) **3** desolvated.

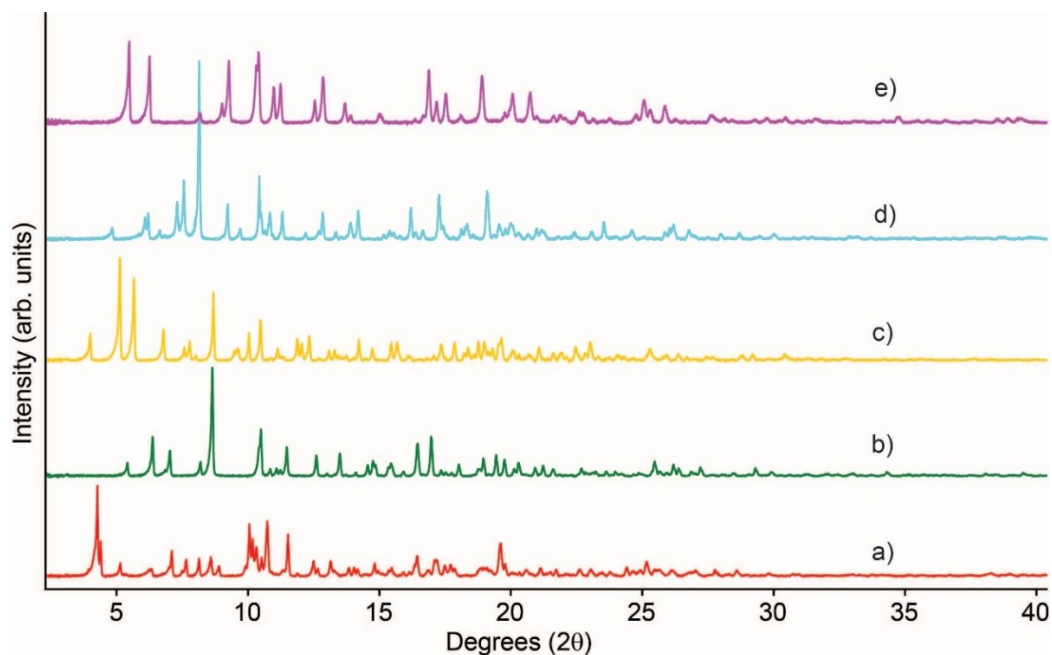


Figure S19. Powder X-ray diffraction patterns of all as-synthesized solvatomorphs (**1a-e**); a) **1a**; b) **1b-DMSO**; c) **1c**; d) **1d**; e) **1e**.

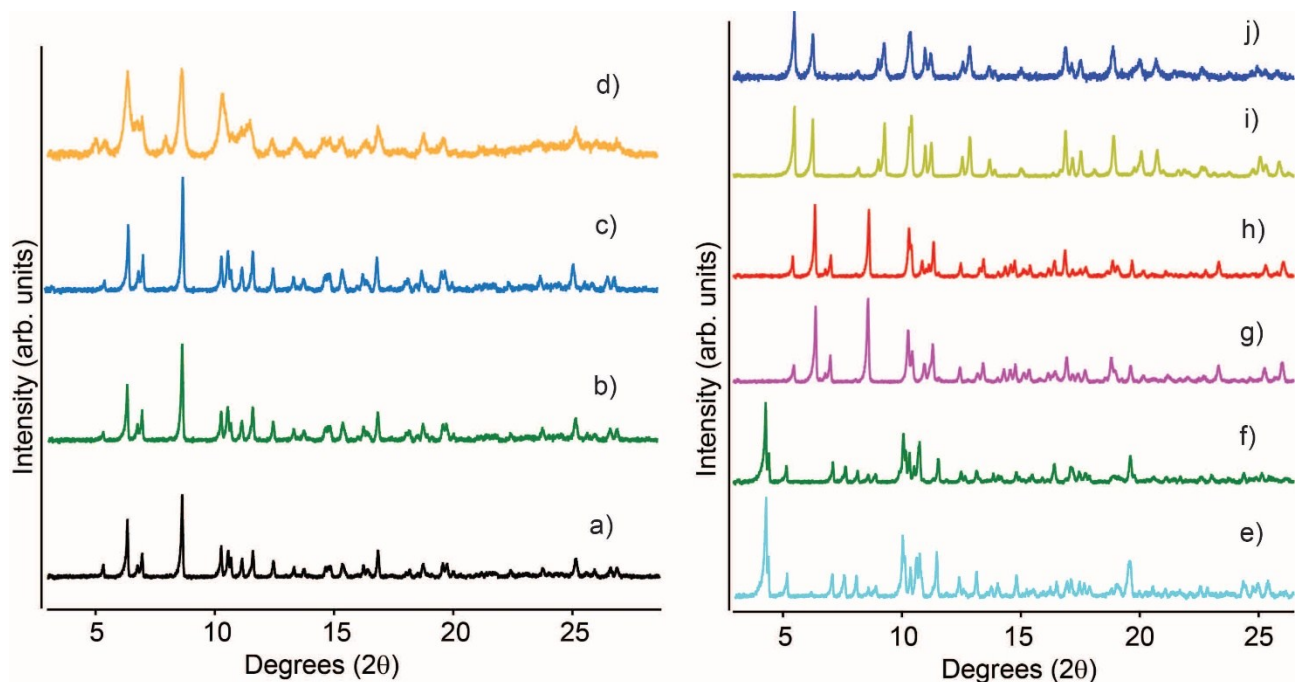


Figure S20. Powder X-ray diffraction patterns of samples of **1a**, **1b** and **1e** after activation and re-solvating in MeOH (a-d) and mother liquor (e-f); a) **1b**-MeOH; b) **1a** activated, then re-solvated in MeOH; c) **1b** activated, then resolvated in MeOH; d) **1e** activated, then resolvated in MeOH; e) **1a** as synthesised; f) **1a** activated, then resolvated in a 1:6 mixture of DMF:MeOH; g) **1b** as synthesised; h) **1b** activated, then resolvated in a 1:6 mixture of DMA:MeOH; i) **1e** as synthesised; j) **1e** activated, then resolvated in acetone.

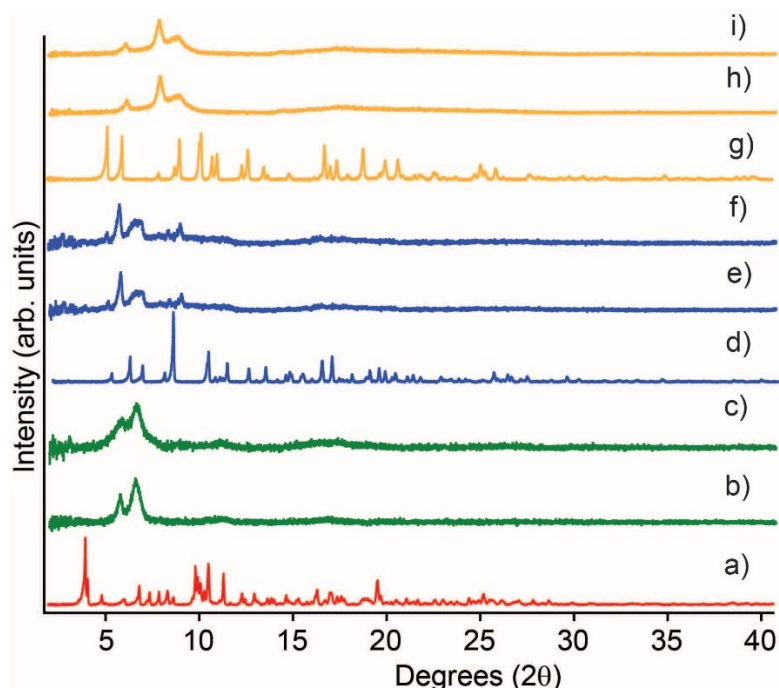


Figure S21. Powder X-ray diffraction patterns comparing the activated and post-adsorption samples of **1a**, **1b** and **1e**; a) **1a** as-synthesised; b) **1a** after activating a 100 °C; c) the activated sample of **1a** post N₂ adsorption; d) **1b** as-synthesised; e) **1b** after activating a 100 °C; f) the activated sample of **1b** post N₂ adsorption; g) **1e** as-synthesised; h) **1e** after activating a 100 °C; i) the activated sample of **1b** post N₂ adsorption.

3. Thermal gravimetric analysis (TGA)

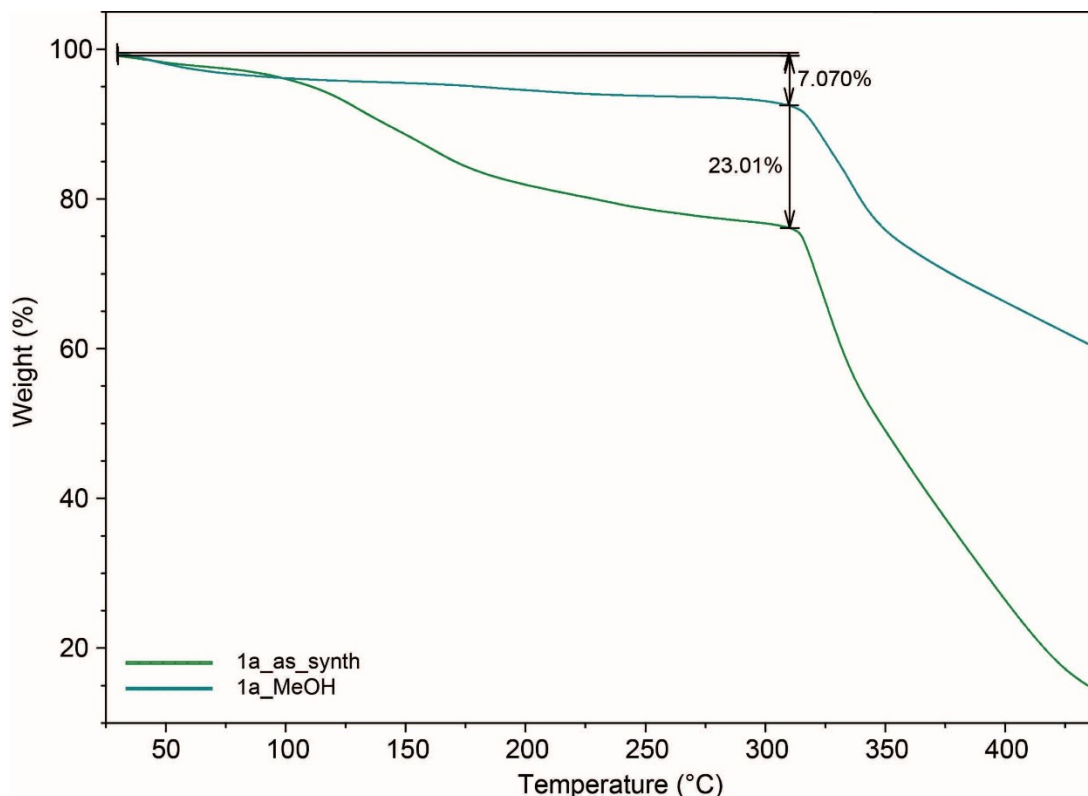


Figure S22. TGA trace overlay of **1a**-as synthesised (green) and **1a**-MeOH (teal). Thermal decomposition of the solids occurs at ca. 310 °C.

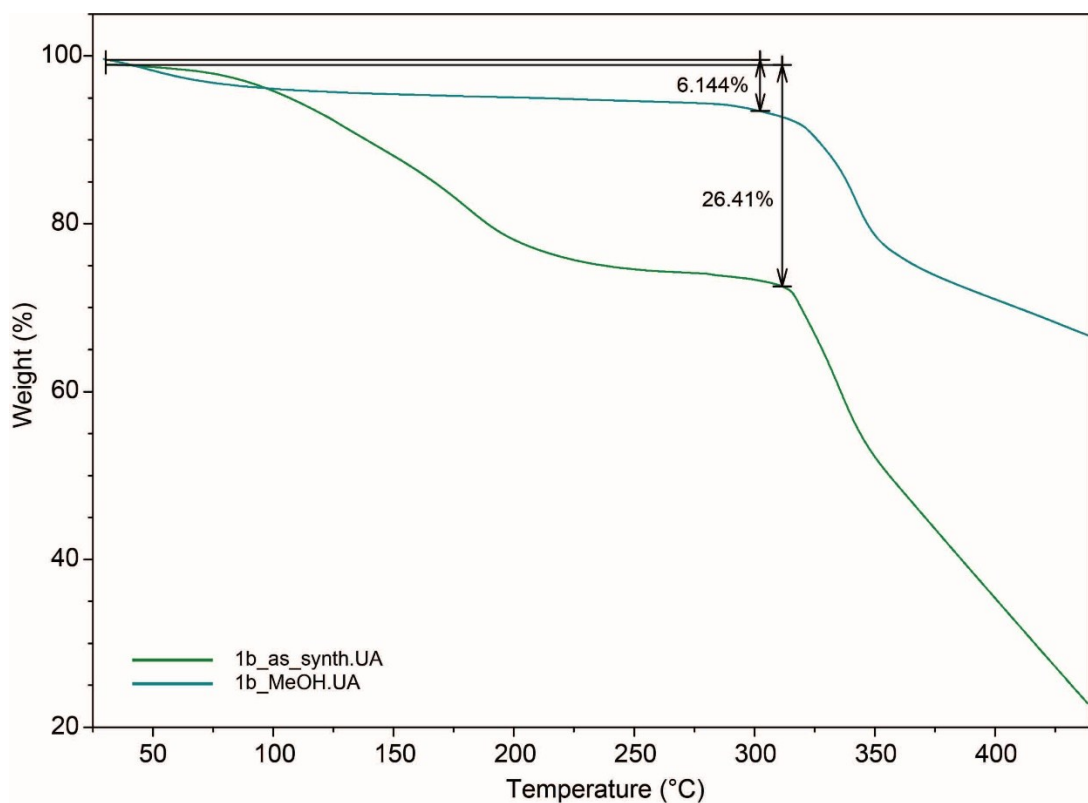


Figure S23. TGA trace overlay of **1b**-as synthesised (**1b**-DMA, green) and **1a**-MeOH (teal). Thermal decomposition of the solids occurs at 300 – 310 °C.

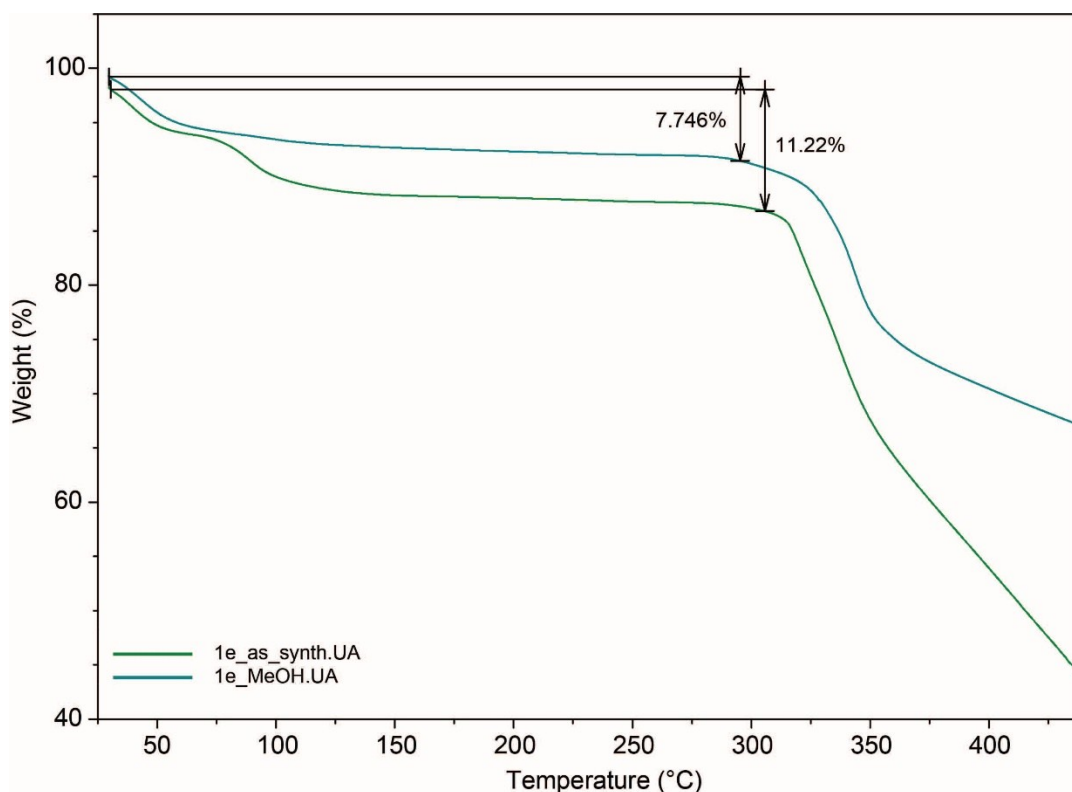


Figure S24. TGA trace overlay of **1e**-as synthesised (**1e**-acetone, green) and **1e**-MeOH (teal). Thermal decomposition of the solids occurs at. 290 – 310 °C.

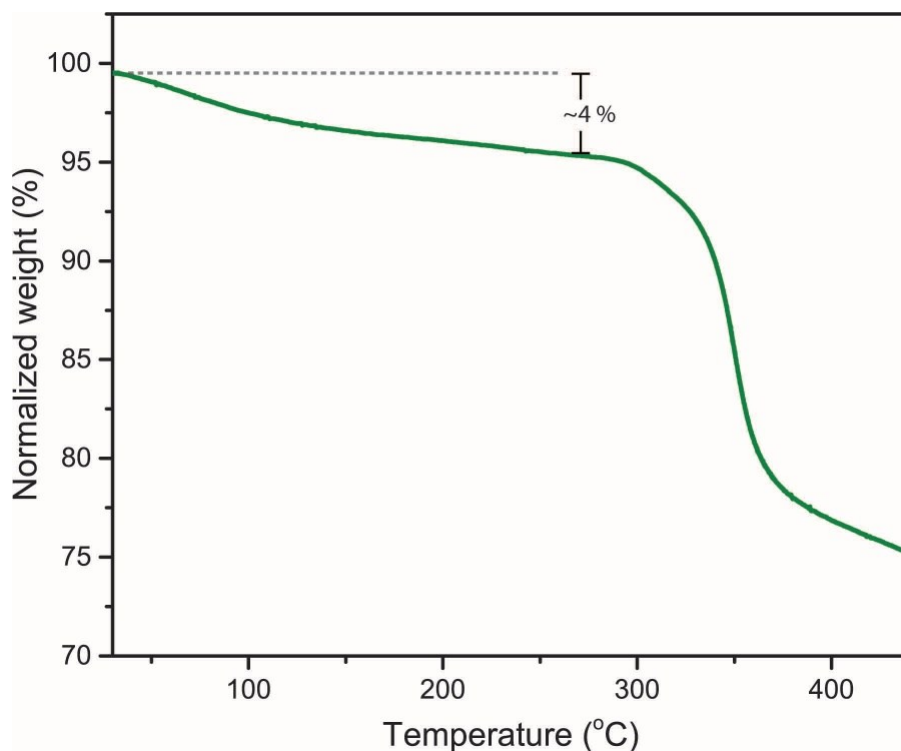


Figure S25. TGA trace of an activated sample (e.g. **1b**) after adsorption analysis. Upon exposure to air, the samples quickly change from deep blue to a light blue colour. Accordingly, a gradual loss of H₂O (4%) is observed which corresponds to the loss of four water molecules per cage. Thermal decomposition of the solid occurs at ca. 300 °C

4. Gas adsorption

Prior to activation, **1a**, **1b** and **1e** were soaked in MeOH (x 7) over a period of 24 h. To verify whether complete exchange of the parent solvent with MeOH had taken place after, samples were digested in DMSO/DCI and analysed by ^1H NMR spectroscopy (figure below).

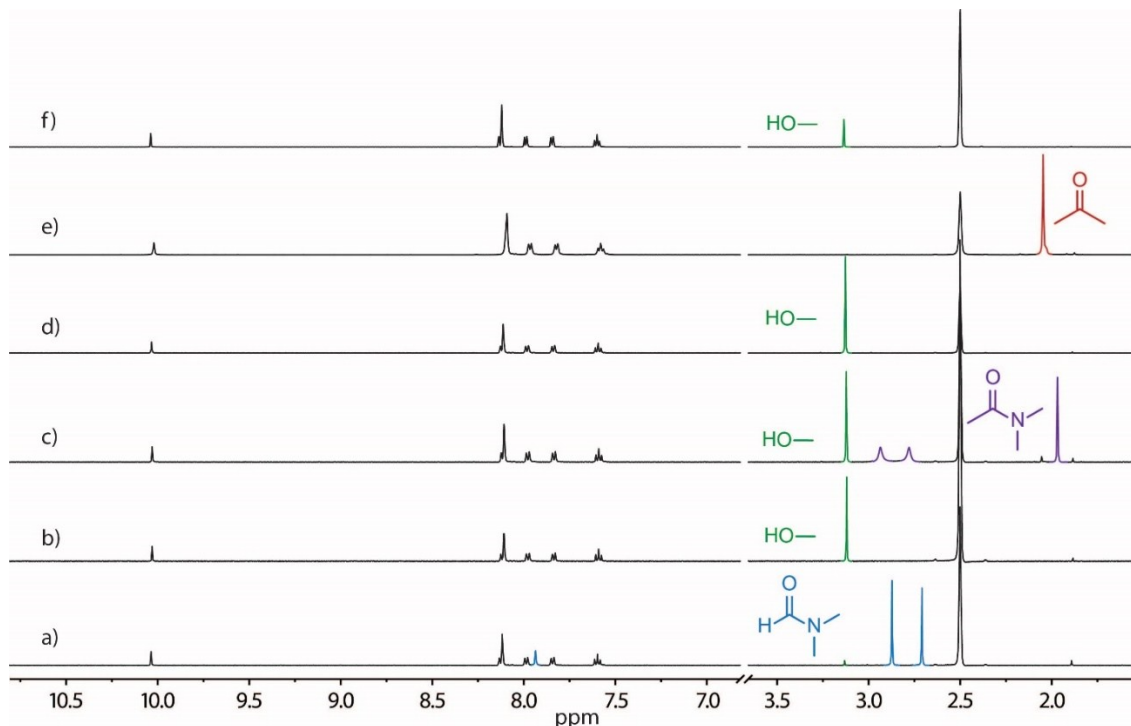


Figure S26. ^1H NMR (500 MHz/DMSO) spectra of digested samples of **1**; a) **1a** as-synthesised (DMF/MeOH); b) **1a** methanol exchanged; c) **1b** as-synthesised (DMA/MeOH); d) **1b** MeOH exchanged; e) **1e** as-synthesised (acetone); e) **1e** MeOH exchanged.

All samples were activated from MeOH at 100 °C under vacuum for 6 hrs. ^1H NMR digestions in DMSO/DCI confirmed complete removal of the solvent (e.g. figure below).

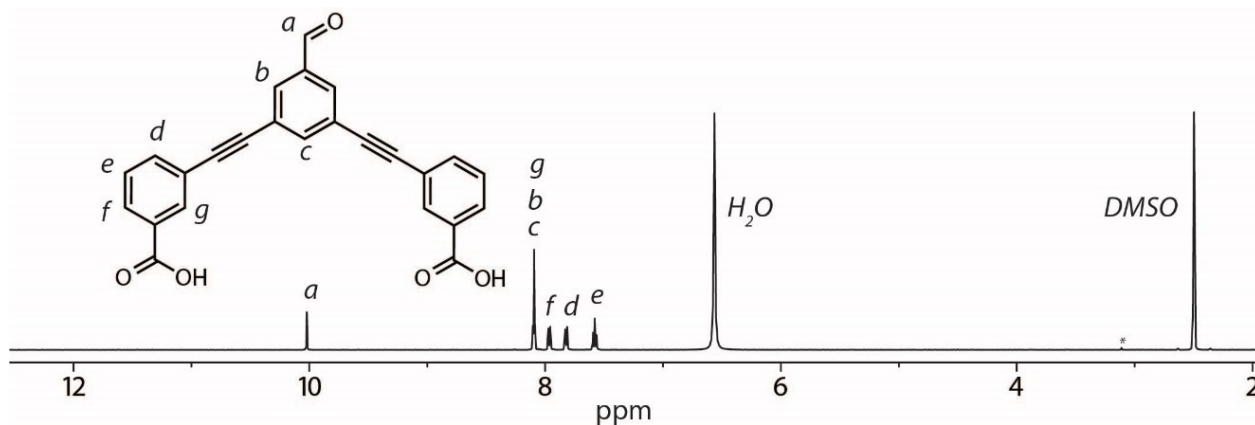


Figure S27. ^1H NMR (500 MHz/DMSO) of a digested sample of **1** after activation from MeOH. * indicates residual MeOH of <0.2%. Further heating under vacuum did not improve the BET surface area of samples of **1**.

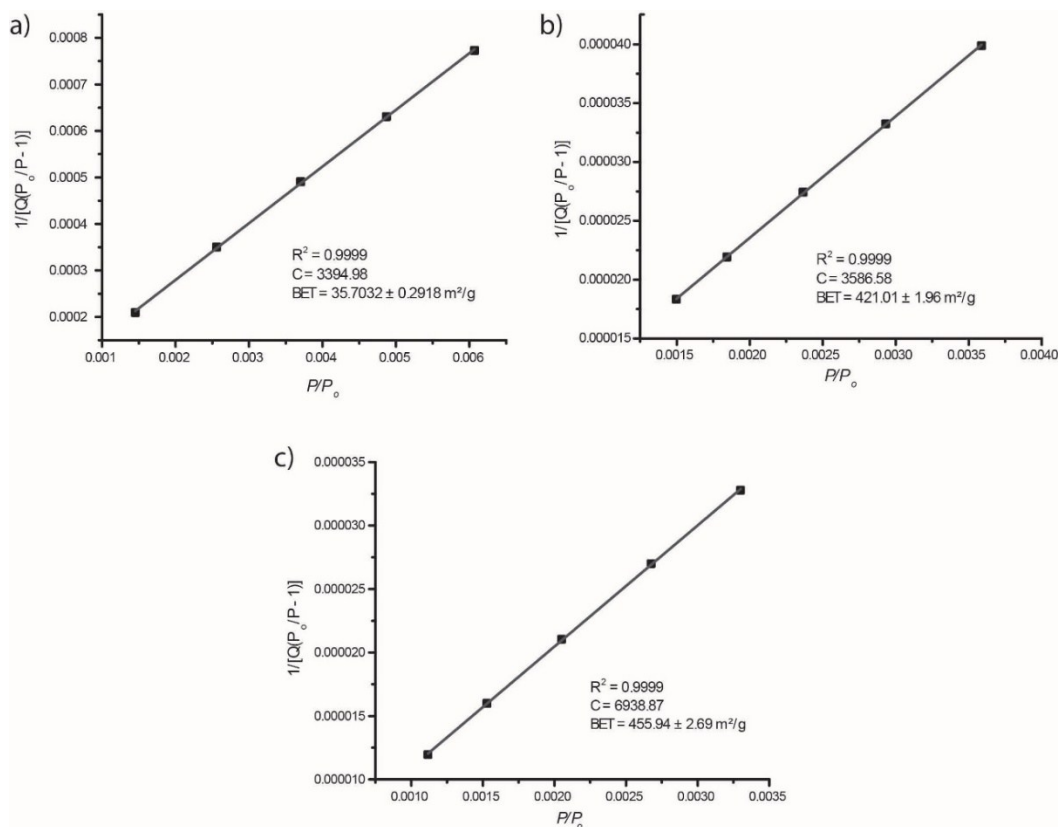


Figure S28. Derivation of the BET surface area from the 77 K N₂ adsorption isotherms for a) **1a**; b) **1b**; c) **1e**.

5. X-ray crystallography

4.1. General methods

Single crystals were mounted in paratone-N oil on a plastic loop. X-ray diffraction data for **1a**, **1b**, **1e**, **2** and **3** were collected at 100(2) K on the MX-1 beamline of the Australian Synchrotron.² X-ray diffraction data for **1c** and **1d** were collected at 150(2) K on an Oxford X-Calibur single crystal diffractometer ($\lambda = 0.7107 \text{ \AA}$). Data sets were corrected for absorption using a multi-scan method, and structures were solved by direct methods using SHELXT³ and refined with SHELXL⁴ and ShelXle⁵ as a graphical user interface. All non-hydrogen atoms were refined anisotropically and hydrogen atoms were included as invariants at geometrically estimated positions. X-ray experimental data is given in Table S2 and S3

3.1.1. Specific refinement details for **1a** and **1c**

Stereochemical restraints for DMF solvent molecules (residue defined as DMF) were generated by the GRADE program using the GRADE Web Server (<http://grade.globalphasing.org>) and applied in the refinement. A GRADE dictionary for SHELXL contains target values and standard deviations for 1,2-distances (DFIX) and 1,3-distances (DANG), as well as restraints for planar groups (FLAT). This help to resolve the disorder of the coordinate DMF solvent molecules in both **1a** and **1c**. All displacements for non-hydrogen atoms were refined anisotropically. The refinement of ADP's for carbon, nitrogen and oxygen atoms was enabled by a combination of similarity restraints (SIMU) and rigid bond restraints (RIGU).⁶ The contribution of the electron density from disordered, pore-bound solvent molecules, which could not be modelled with discrete atomic positions were handled using the SQUEEZE⁷ routine in PLATON,⁸ which strongly improved all figures of merit (FOM).

3.1.2. Specific refinement details for **1b**

Stereochemical restraints for DMSO solvent molecules (residue defined as SUL) were generated by the GRADE program using the GRADE Web Server (<http://grade.globalphasing.org>) and applied in the refinement. This helped to refine and resolve the disorder about the coordinated DMSO ligands. All displacements for non-hydrogen atoms were refined anisotropically. The refinement of ADP's for

carbon, nitrogen and oxygen atoms was supported by a combination of similarity restraints (SIMU) and rigid bond restraints (RIGU).⁶ The contribution of the electron density from disordered, pore-bound solvent molecules, which could not be modelled with discrete atomic positions were handled using the SQUEEZE⁷ routine in PLATON,⁸ which strongly improved all figures of merit (FOM).

3.1.5. Specific refinement details for **1d**

Stereochemical restraints for DMA solvent molecules (residue defined as DMA) were generated by the GRADE program using the GRADE Web Server (<http://grade.globalphasing.org>) and applied in the refinement. This helped to resolve the disorder of the coordinated DMA molecules. All displacements for non-hydrogen atoms were refined anisotropically. The refinement of ADP's for carbon, nitrogen and oxygen atoms was supported by similarity restraints (SIMU).⁶ The contribution of the electron density from disordered, pore-bound solvent molecules, which could not be modelled with discrete atomic positions were handled using the SQUEEZE⁷ routine in PLATON,⁸ which strongly improved all figures of merit (FOM).

3.1.4. Specific refinement details for **1e**

All displacements for non-hydrogen atoms were refined anisotropically. The refinement of ADP's for carbon, nitrogen and oxygen atoms was supported by similarity restraints (SIMU).⁶ The contribution of the electron density from disordered, pore-bound solvent molecules, which could not be modelled with discrete atomic positions were handled using the SQUEEZE⁷ routine in PLATON,⁸ which strongly improved all figures of merit (FOM).

3.1.6. Specific refinement details for **2**

All displacements for non-hydrogen atoms were refined anisotropically. The refinement of ADP's for carbon, nitrogen and oxygen atoms was supported by similarity restraints (SIMU).⁶ The contribution of the electron density from disordered, pore-bound solvent molecules, which could not be modelled with discrete atomic positions were handled using the SQUEEZE⁷ routine in PLATON,⁸ which strongly improved all figures of merit (FOM).

3.1.7. Specific refinement details for **3**

Stereochemical restraints for DMF solvent molecules (residue defined as DMF) were generated by the GRADE program using the GRADE Web Server (<http://grade.globalphasing.org>) and applied in the refinement. All displacements for non-hydrogen atoms were refined anisotropically. The refinement of ADP's for carbon, nitrogen and oxygen atoms was supported by similarity restraints (SIMU).⁶ The contribution of the electron density from disordered, pore-bound solvent molecules, which could not be modelled with discrete atomic positions were handled using the SQUEEZE⁷ routine in PLATON,⁸ which strongly improved all figures of merit (FOM).

Table S2: X-ray experimental data for **1a**, **1b**, **1c** and **1d**

Compound	1a	1b	1c	1d
CCDC number	1969623	1969620	1969621	1969625
Empirical formula	C ₂₁₈ H ₁₃₈ Cu ₈ N ₆ O ₄₈	C ₁₀₈ H ₇₂ Cu ₄ O ₂₄ S ₄	C ₅₃ H ₃₁ Cu ₂ NO ₁₂	C ₁₁₆ H ₈₄ Cu ₄ N ₄ O ₂₄
Formula weight	4117.66	2136.05	1000.87	2172.03
Crystal system	Triclinic	Monoclinic	Monoclinic	Monoclinic
Space group	<i>P</i> -1	<i>C</i> 2/ <i>c</i>	<i>I</i> 2/ <i>m</i>	<i>P</i> 2 ₁ / <i>c</i>
<i>a</i> (Å)	13.914(3)	14.151(3)	25.8186(7)	14.0177(5)
<i>b</i> (Å)	20.891(4)	32.563(7)	22.6806(6)	28.7314(8)
<i>c</i> (Å)	21.446(4)	26.766(5)	27.2079(6)	17.0738(6)
α (°)	71.94(3)	90	90	90
β (°)	87.87(3)	102.26	109.690(3)	110.611(4)
γ (°)	81.20(3)	90	90	90
Volume (Å ³)	5857(2)	12052(4)	15000.9(7)	6436.3(4)
<i>Z</i>	1	4	8	2
Density (calc.) (Mg/m ³)	1.167	1.177	0.886	1.121
Absorption coefficient (mm ⁻¹)	0.780	0.827	0.608	0.714

F(000)	2104	4368	4080	2232
Crystal size (mm ³)	0.10x0.04x0.03	0.2x0.07x0.05	0.31x0.23 x0.22	0.31x0.18x0.08
θ range for data collection (°)	0.999 to 23.257	1.251 to 23.260	3.346 to 27.771	3.328 to 28.199
Reflections collected	57266	56711	56310	57672
Observed reflections [R(int)]	15206 [0.0436]	8490 [0.0824]	15144 [0.0596]	13776 [0.0539]
Goodness-of-fit on F ²	1.139	1.053	1.035	1.028
R ₁ [$I > 2\sigma(I)$]	0.0525	0.0714	0.0758	0.0550
wR ₂ (all data)	0.1633	0.2406	0.2289	0.1518
Largest diff. peak and hole (e.Å ⁻³)	0.902 and -0.516	1.088 and -0.505	0.975 and -1.269	0.715 and -0.376
Data / restraints / parameters	15206 / 1085 / 1321	8490 / 1092 / 695	15144 / 816 / 688	13776 / 648 / 761

Table S3: X-ray experimental data for **1e**, **2** and **3**

Compound	1e	2	3
CCDC number	1969624	1969619	1969622
Empirical formula	C ₁₀₆ H ₆₀ Cu ₄ O ₂₄	C ₁₄₀ H ₁₀₄ Cu ₄ N ₈ O ₂₀	C ₁₆₈ H ₁₂₄ Cu ₄ N ₁₂ O ₂₀
Formula weight	1971.70	2472.47	2884.94
Crystal system	Monoclinic	Triclinic	Monoclinic
Space group	<i>C2/m</i>	<i>P-1</i>	<i>P2₁/n</i>
<i>a</i> (Å)	19.687 (4)	14.987(3)	20.979(4)
<i>b</i> (Å)	28.163 (6)	16.858(3)	21.168(4)
<i>c</i> (Å)	10.475 (2)	17.478(4)	23.760(5)
α (°)	90	116.53(3)	90
β (°)	97.91 (3)	107.31(3)	108.37(3)
γ (°)	90	93.21(3)	90
Volume (Å ³)	5753 (2)	3678.4(16)	10014(4)
Z	2	1	2
Density (calc.) (Mg/m ³)	1.138	1.116	0.957
Absorption coefficient (mm ⁻¹)	0.791	0.631	0.472
F(000)	2008	1276	2984
Crystal size (mm ³)	0.11x0.08x0.07	0.15x0.13x0.09	0.05x0.04x0.02
θ range for data collection (°)	1.963 to 24.111	1.384 to 25.681	1.131 to 24.413
Reflections collected	31901	46313	115160
Observed reflections [R(int)]	4464 [0.0286]	12313 [0.0260]	15671 [0.1473]
Goodness-of-fit on F ²	1.054	1.027	1.024
R ₁ [$I > 2\sigma(I)$]	0.0429	0.0431	0.1220
wR ₂ (all data)	0.1216	0.1324	0.3929
Largest diff. peak and hole (e.Å ⁻³)	0.566, -0.508	0.447 and -1.005	1.998 and -0.869
Data / restraints / parameters	4464/ 222 / 315	12313 / 0 / 781	15671 / 723 / 926

5.2. Thermal ellipsoid plots

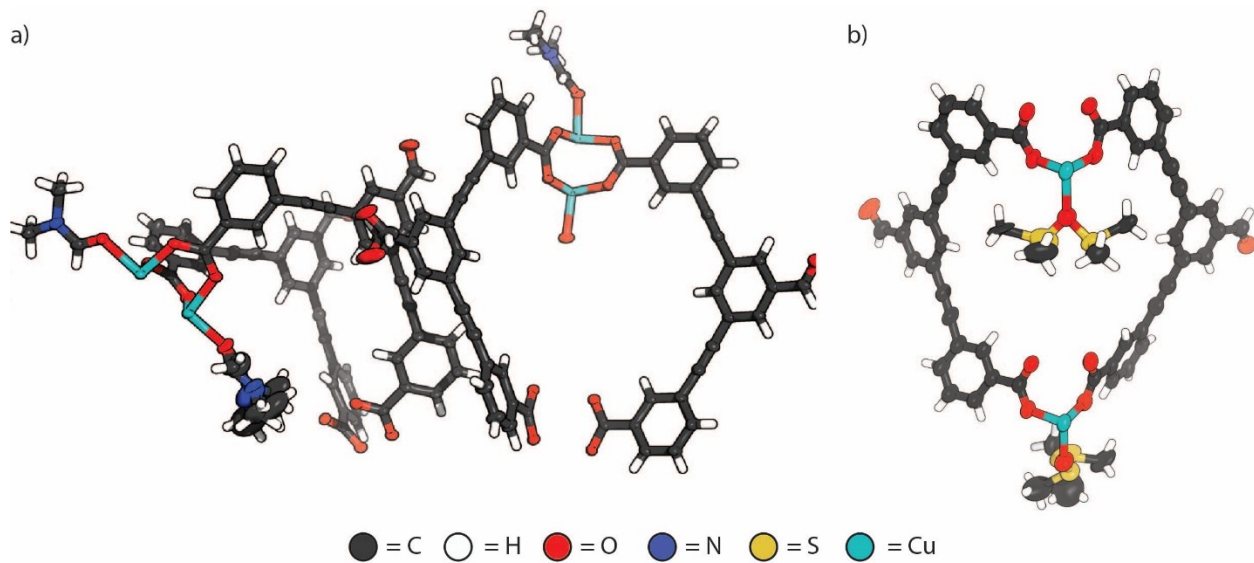


Figure S29. The asymmetric unit of the X-ray structures of a) **1a** and b) **1b** with all non-hydrogen atoms shown as ellipsoids at the 50% probability level.

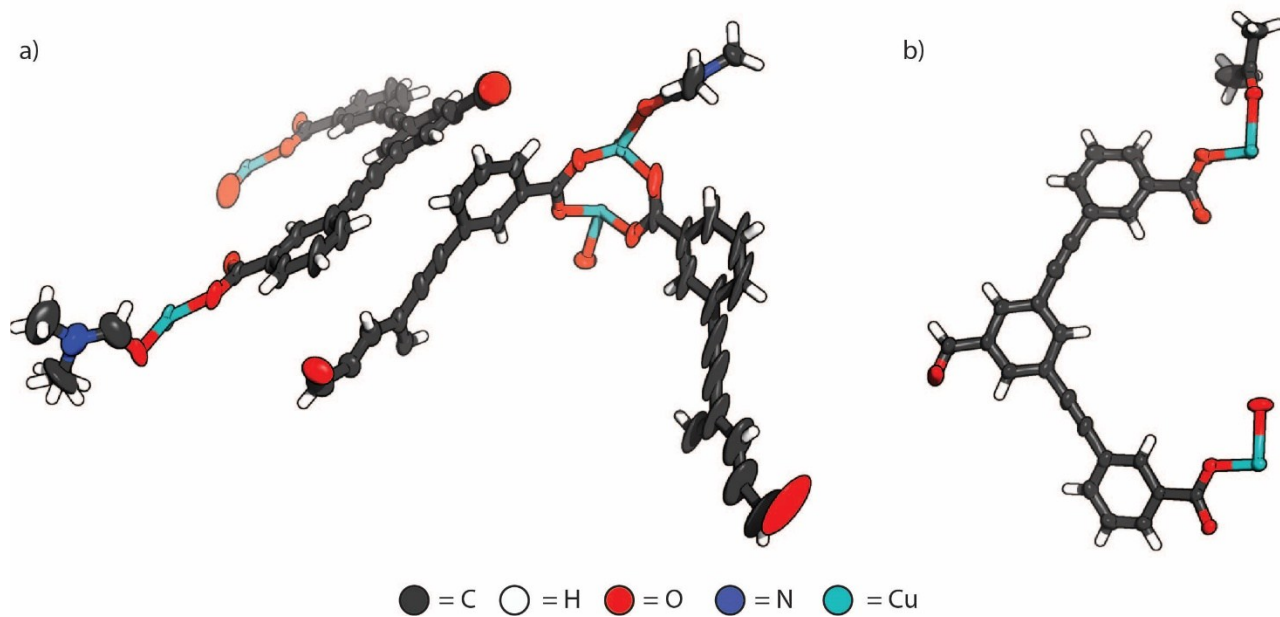


Figure S30. The asymmetric unit of the X-ray structures of a) **1c** and b) **1e** with all non-hydrogen atoms shown as ellipsoids at the 50% probability level.

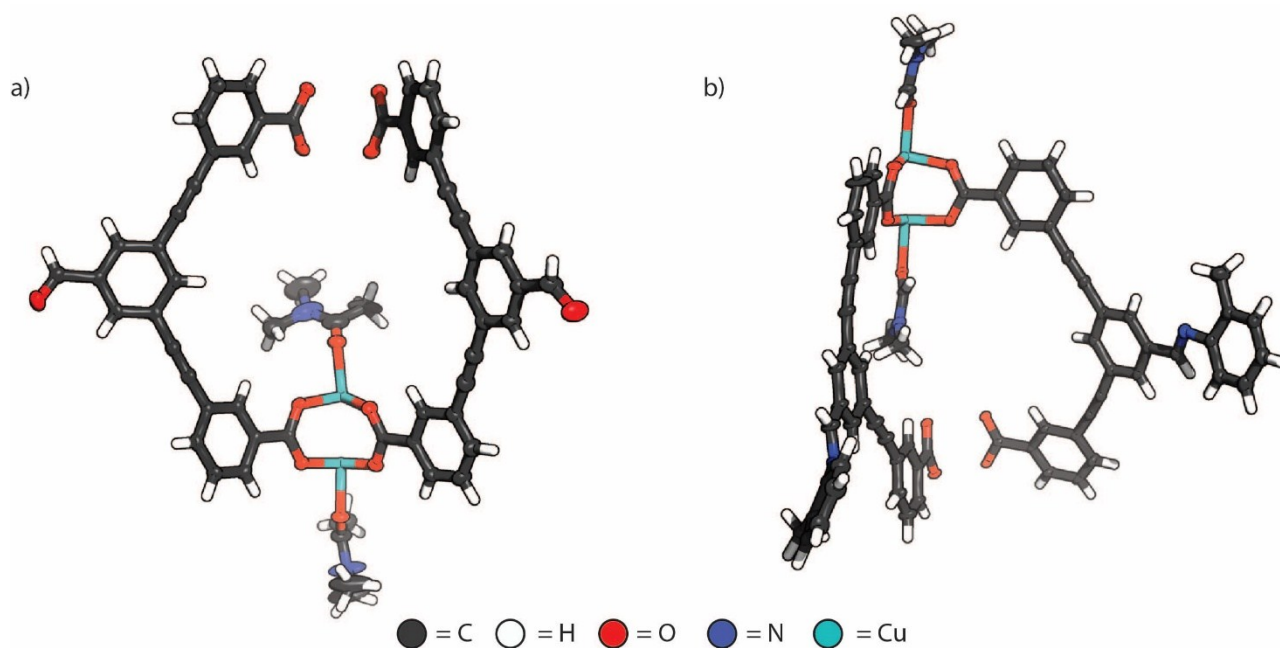


Figure S31. The asymmetric unit of the X-ray structures of a) **1d** and b) **2** with all non-hydrogen atoms shown as ellipsoids at the 50% probability level.

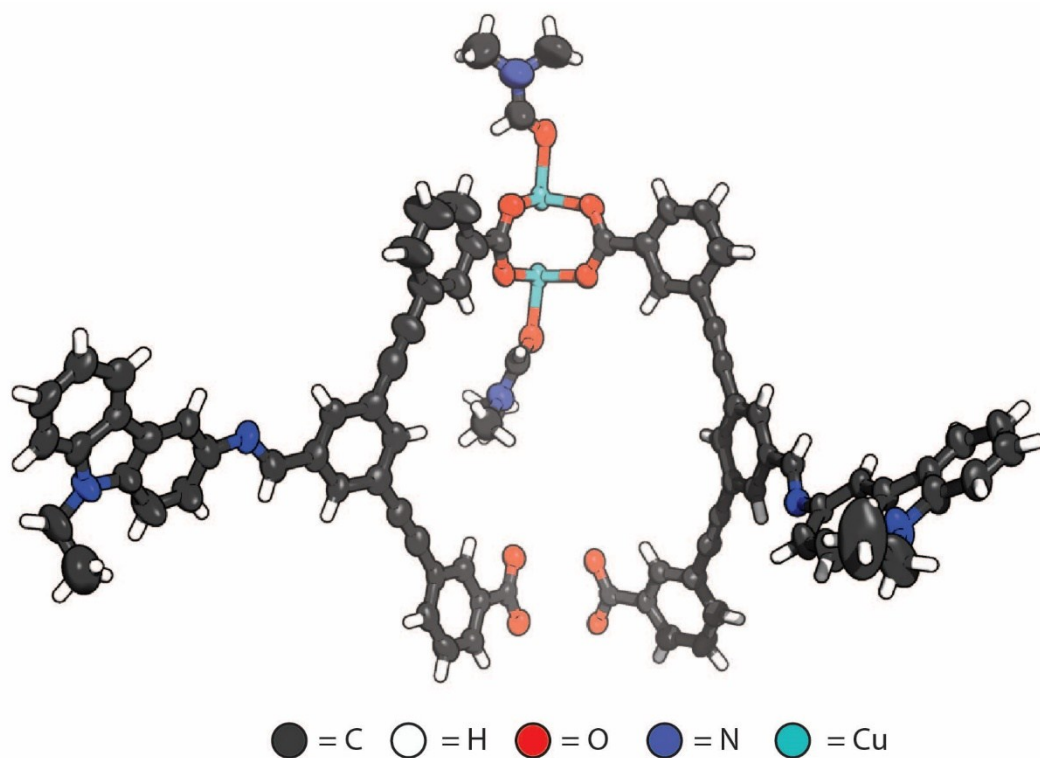


Figure S32. The asymmetric unit of the X-ray structures of **3** with all non-hydrogen atoms shown as ellipsoids at the 50% probability level.

5.3. Additional information on 1a-e

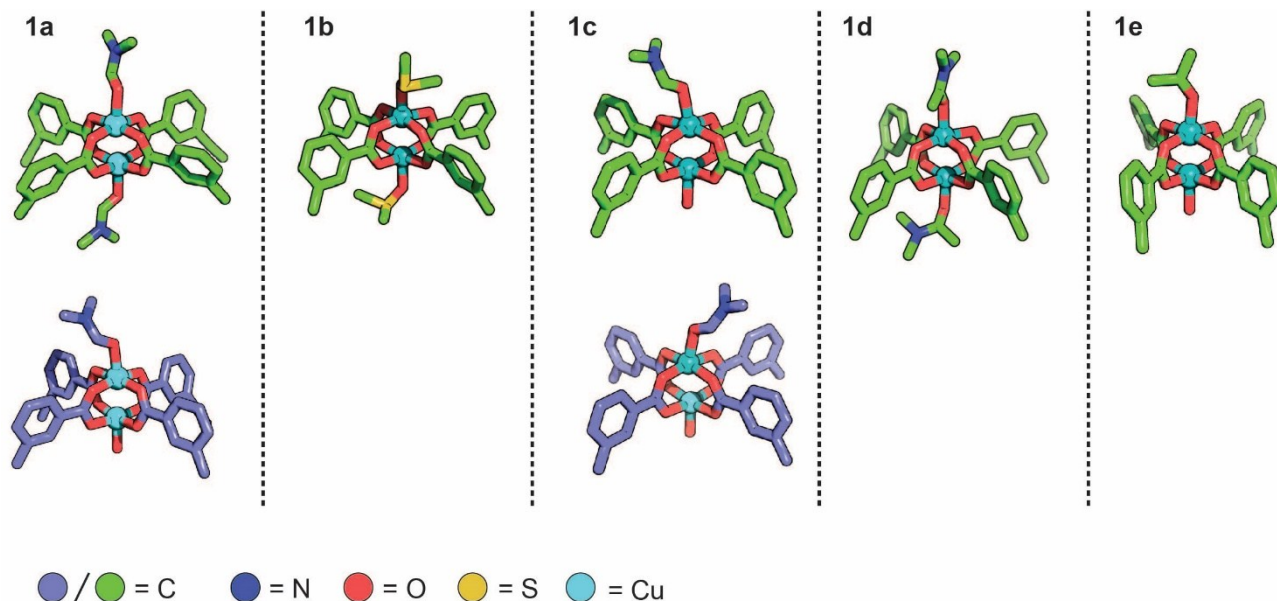


Figure S33. The coordination sphere of phases **1a-e**. **1a** and **1c** have either chemically (**1a**) or crystallographically (**1c**) unique paddle-wheel centres and are thus shown in two colours.

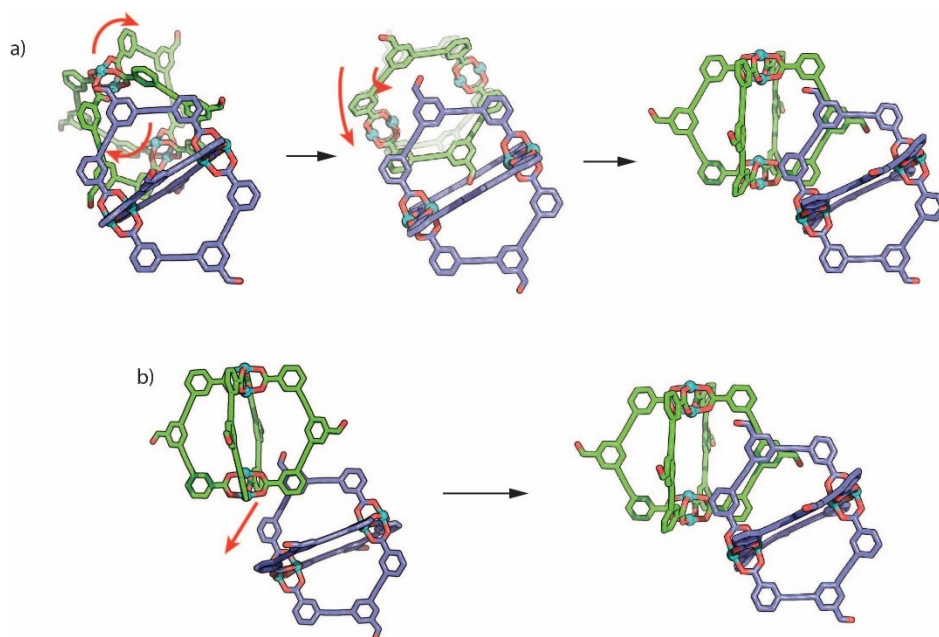


Figure S34. A scheme depicting the cage-to-cage relationship in the packing of **1c** and **1d**, along with a possible mechanism behind solid-state transformations to **1b** that occurs upon washing these samples with MeOH a) **1c** transforming to **1b**; **1e** transforming to **1b**. For **1c**, we propose that the transformation to **1b** occurs through two rotations about one cage molecule with respect to the other. For **1d**, we suggest a sliding motion about the ligand backbone of adjacent cage molecules (Fig. S27).

6. Lattice energy calculations

Lattice energy calculations for each of the polymorphs were calculated based on the periodic density functional theory (DFT) as implemented in the software package VASP 5.4.4.⁹ The initial model for the DFT simulations were taken from the experimental CIF files where the solvent molecules are removed, and the disorder atoms are refined. A unit cell was employed for all the polymorph structures except for polymorph **1c**, a primitive cell is used. It is well-known that standard DFT methods based on generalized gradient approximation do not fully account for the long-range dispersion interactions and hence we included the dispersion corrections using DFT-D3 method.¹⁰ Electron exchange and correlation were described using the generalized gradient approximation Perdew, Burke, and Ernzerhof (PBE)¹¹ form and the projector-augmented wave potentials were used to treat core and valence electrons.¹² In all cases, we used a plane-wave kinetic energy cutoff of 600 eV and a Gamma-point mesh for sampling the Brillouin zone. The ionic coordinates and cell parameters were fully relaxed until the Hellman-Feynman ionic forces were less than 0.01 eV/Å.

Table S4 Absolute lattice energies for polymorphic structures of **1a-e**

Structure	Lattice energy (kJ/mol)
1a	-363.768
1b	-386.109
1c	-279.820
1d	-317.136
1e	-370.838

Table S5: DFT optimised lattice parameters of phases **1a-e**. The values in the bracket refers to the experimental value.

Structures	DFT optimised Lattice parameter						% change in lattice cell parameters with respect to experimental values		
	a (Å)	b (Å)	c (Å)	α (°)	β (°)	γ (°)	a (Å)	b (Å)	c (Å)
1a	12.423 (13.914)	21.258 (20.891)	20.762 (21.446)	66.47 (71.94)	92.16 (87.87)	78.80 (81.20)	10.71	-1.75	3.19
1b	14.068 (14.151)	30.961 (32.563)	26.892 (26.766)	90 (90)	100.91 (102.26)	90 (90)	0.58	4.9	-0.47
1c	19.262 (19.025)	18.478 (19.025)	24.185 (27.208)	59.35 (60.89)	60.67 (60.89)	77.13 (73.17)	-1.24	2.87	11.11
1d	14.173 (14.017)	28.161 (28.731)	16.146 (17.073)	90 (90)	110.63 (110.61)	90 (90)	-1.11	1.98	5.43
1e	20.823 (19.687)	25.775 (28.163)	10.402 (10.475)	90 (90)	104.87 (97.91)	90 (90)	-5.77	8.45	0.70

Table S6: Density of the structures after DFT optimisation with solvent removed and the corresponding lattice energy. The values in the bracket refers to the experimental density with the solvent molecule removed.

Structures	Density (g/cm ³)	Lattice Energy (kJ/mol)
1a	1.238 (1.167)	-363.768
1b	1.053 (1.005)	-386.109
1c	0.938 (0.807)	-279.820
1d	1.004 (0.941)	-317.136
1e	1.122 (1.053)	-370.838

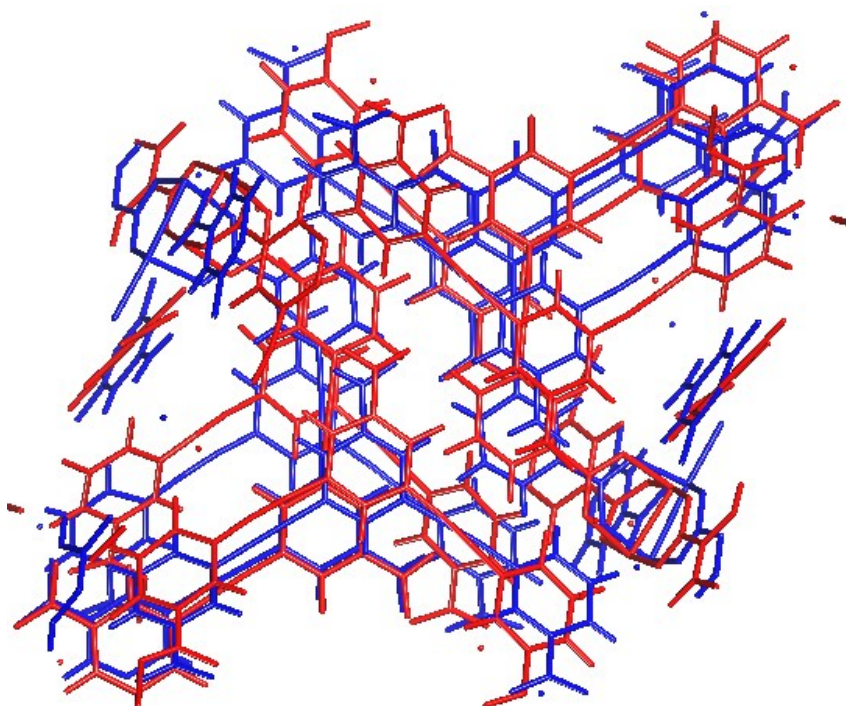


Figure S35. Overlay of polymorph **1a** before (blue) and after DFT optimisation (red) with a RMSD of 4.15 Å.

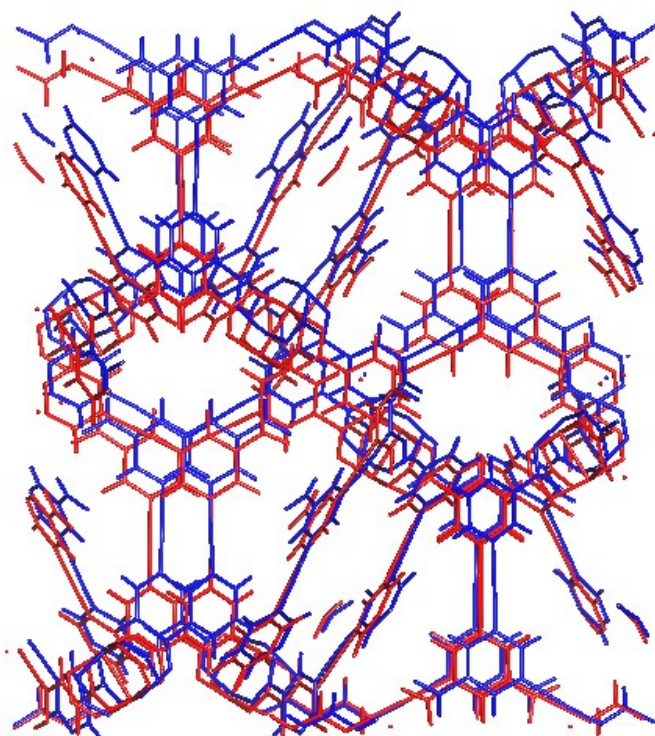


Figure S36. Overlay of polymorph **1b** before (blue) and after DFT optimization (red) with a RMSD of 2.98 Å.

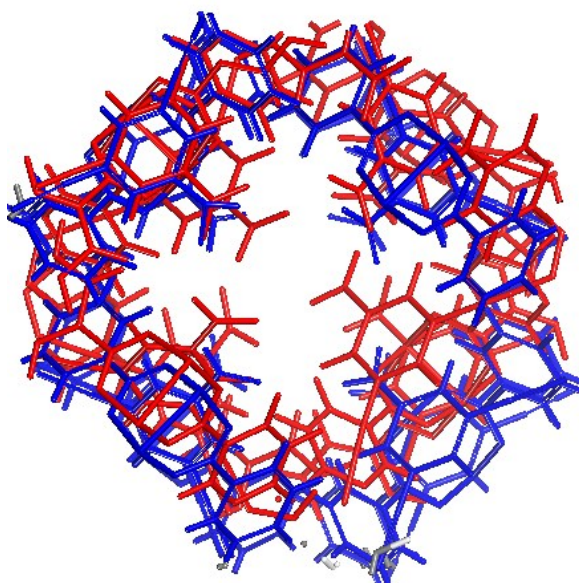


Figure S37. Overlay of polymorph **1c** before (blue) and after DFT optimization (red) with a RMSD of 5.46 Å.

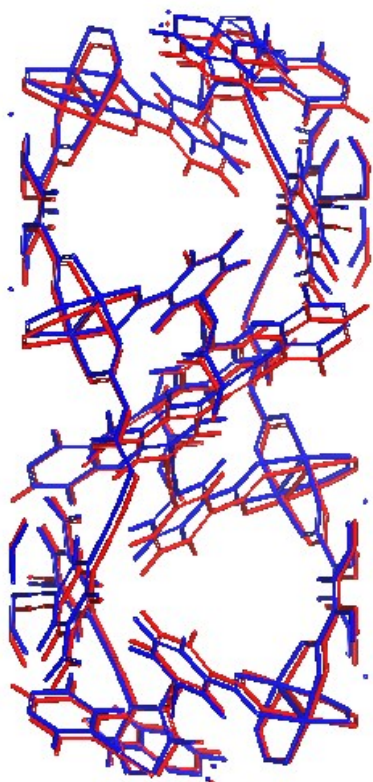


Figure S38. Overlay of polymorph **1d** before (blue) and after DFT optimisation (red) with a RMSD of 0.725 Å.

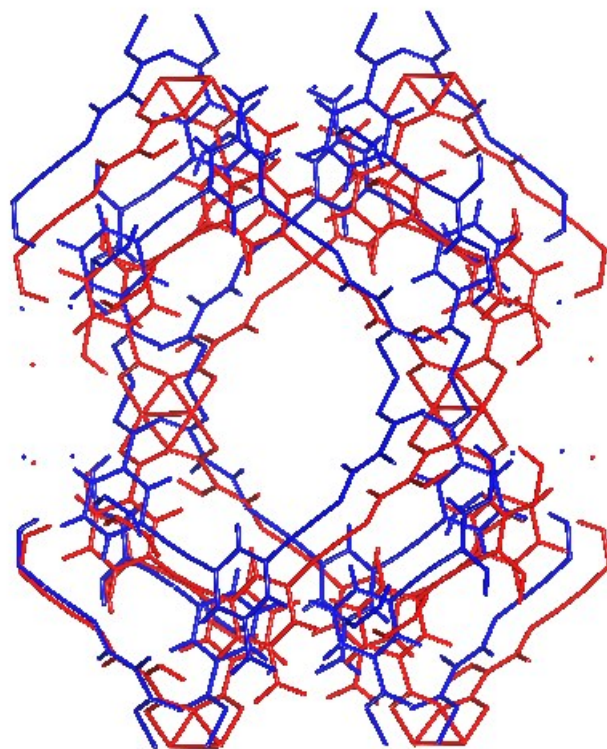


Figure S39. Overlay of polymorph **1e** before (blue) and after DFT optimisation (red) with a RMSD of 1.523 Å.

7. References

- 1 V. Brega, M. Zeller, Y. He, H. Peter Lu and J. K. Klosterman, *Chem. Commun.*, 2015, **51**, 5077–5080.

- 2 N. P. Cowieson, D. Aragao, M. Cliff, D. J. Ericsson, C. Gee, S. J. Harrop, N. Mudie, S. Panjikar, J. R. Price, A. Riboldi-Tunncliffe, R. Williamson and T. Caradoc-Davies, *J. Synchrotron Radiat.*, 2015, **22**, 187–190.
- 3 G. M. Sheldrick, *Acta Crystallogr. Sect. A*, 2015, **71**, 3–8.
- 4 G. M. Sheldrick, *Acta Crystallogr. Sect. C*, 2015, **71**, 3–8.
- 5 C. B. Hubschle, G. M. Sheldrick and B. Dittrich, *J. Appl. Crystallogr.*, 2011, **44**, 1281–1284.
- 6 A. Thorn, B. Dittrich and G. M. Sheldrick, *Acta Crystallogr. Sect. A*, 2012, **68**, 448–451.
- 7 A. Spek, *Acta Crystallogr. Sect. C*, 2015, **71**, 9–18.
- 8 A. Spek, *Acta Crystallogr. Sect. D*, 2009, **65**, 148–155.
- 9 G. Kresse, J. Hafner, *Phys. Rev. B*, 1993, **48**, 13115-13118.
- 10 S. Grimme, S. Ehrlich, L. Goerigk, *J. Comp. Chem.*, 2011, **32**, 1456-1465
- 11 J. P. Perdew, K. Burke, M. Ernzerhof, *Phys. Rev. Lett.*, 1996, **77**, 3865-3868.
- 12 G. Kresse, D. Joubert, *Phys. Rev. B*, 1999, **59**, 1758-1775